

# Nonlinear Schwinger mechanism in QCD, and Fredholm alternatives theorem

M. N. Ferreira<sup>1,2</sup> and J. Papavassiliou<sup>3,4</sup>

<sup>1</sup>*School of Physics, Nanjing University, Nanjing, Jiangsu 210093, China*

<sup>2</sup>*Institute for Nonperturbative Physics, Nanjing University,  
Nanjing, Jiangsu 210093, China*

<sup>3</sup>*Department of Theoretical Physics and IFIC, University of Valencia and CSIC,  
E-46100, Valencia, Spain*

<sup>4</sup>*ExtreMe Matter Institute EMMI, GSI,  
Planckstrasse 1, 64291, Darmstadt, Germany*

## Abstract

We present a novel implementation of the Schwinger mechanism in QCD, which fixes uniquely the scale of the effective gluon mass and streamlines considerably the procedure of multiplicative renormalization. The key advantage of this method stems from the nonlinear nature of the dynamical equation that generates massless poles in the longitudinal sector of the three-gluon vertex. An exceptional feature of this approach is an extensive cancellation involving the components of the integral expression that determines the gluon mass; it is triggered once the Schwinger-Dyson equation of the pole-free part of the three-gluon vertex has been appropriately exploited. It turns out that this cancellation is driven by the so-called Fredholm alternatives theorem, which operates among the set of integral equations describing this system. Quite remarkably, in the linearized approximation this theorem enforces the exact masslessness of the gluon. Instead, the nonlinearity induced by the full treatment of the relevant kernel evades this theorem, allowing for the emergence of a nonvanishing mass. The numerical results obtained from the resulting equations are compatible with the lattice findings, and may be further refined through the inclusion of the remaining fundamental vertices of the theory.

## I. INTRODUCTION

As is well-known, the gauge symmetry of the classical Yang-Mills action [1–4] prohibits the inclusion of a mass term  $m^2 A_\mu^a A^{a\mu}$  for the gauge field  $A_\mu^a$ , and this prohibition persists after the gauge-fixing through the Faddeev-Popov procedure [5] has been carried out, due to the residual Becchi-Rouet-Stora-Tyutin (BRST) symmetry [6–8]. Moreover, symmetry-preserving regularization schemes, such as dimensional regularization [9, 10], prevent the generation of a mass term at any finite order in perturbation theory. Nevertheless, as has been argued over four decades ago [11], a non-perturbative effective gluon mass may be generated through the non-Abelian realization of the Schwinger mechanism (SM) [12, 13]. This dynamical scenario has received particular attention over the years, becoming an integral part of the intense activity associated with the emergence of a mass gap in the gauge sector of QCD [14–53].

In its original formulation, the SM is based on the fundamental observation that a mass for a vector meson may be generated, without clashing with the gauge symmetry of the action, if the corresponding vacuum polarization develops a pole with positive residue ( $m^2$ ) at zero-momentum transfer [12, 13]. In that case, the gluon propagator,  $\Delta(q)$ , saturates to a fixed value at the origin, namely  $\Delta^{-1}(0) = m^2$ , such that the residue of the pole plays the role of an effective mass.

The implementation of this basic idea in the context of Yang-Mills theories, in general, and in the gauge sector of QCD in particular, is technically rather complicated. Specifically, the required pole is provided by the propagator  $\delta^{ab}/q^2$  of a massless color-carrying scalar bound state, formed out of the fusion of a pair of gluons [11, 14, 15, 54–59]. The amplitude for the formation of such a pole, denoted by  $\mathbb{B}(r)$ , is governed by a homogeneous Bethe-Salpeter equation (BSE). The existence of a nontrivial solution for  $\mathbb{B}(r)$  endows the three-gluon vertex with a longitudinally coupled pole [55–59], which is transmitted to the Schwinger-Dyson equation (SDE) [51, 53, 57, 60–74] that governs the momentum evolution of the gluon propagator, triggering the SM. In the limit  $q \rightarrow 0$ , this SDE expresses the effective gluon mass as an integral involving  $\mathbb{B}(r)$ . In addition, the Ward identity (WI) satisfied by the three-gluon vertex is modified by an amount controlled by the so-called “*displacement function*” [59, 75, 76], denoted by  $\mathbb{C}(r)$ , which is intimately connected to  $\mathbb{B}(r)$ .

Even though considerable advances have been made in our understanding of the dynam-

ical scenario outlined above, the treatments presented in the literature leave certain key questions unanswered. First, in the linearized version of the BSE studied thus far, the scale of the solutions for  $\mathbb{B}(r)$  remains undetermined [55–59]; thus, the value of the gluon mass is adjusted from the saturation point of the gluon propagator obtained in lattice simulations [77–94]. Second, the integral expression furnishing the mass is multiplied by  $Z_3$ , the renormalization constant of the three-gluon vertex. As a result, the full treatment of the gluon mass equation requires the implementation of multiplicative renormalization at a non-perturbative level; however, the numerical evaluation of this integral has been carried out by simply setting  $Z_3 = 1$  [40, 55–57, 59, 95].

In the present work we report significant progress towards the self-consistent resolution of the open questions mentioned above. The main points of this analysis may be summarized as follows.

(i) The BSE governing  $\mathbb{B}(r)$  is made nonlinear, by including a term cubic in  $\mathbb{B}$ , not considered in previous studies [55–59, 95]. Quite interestingly, the quadratic part of this dependence on  $\mathbb{B}$  is absorbed into a constant denoted by  $\omega$ ; as a result, the total contribution of this term to the BSE is a factor of the form  $\omega \mathbb{B}(r)$ . Consequently, the resulting integral equation may still be treated as an eigenvalue problem, exactly as was done in the past with the linear BSE. The presence of this novel term determines the scale of the solutions up to an overall sign; since the basic quantities of interest, such as the gluon mass and the displacement function, depend quadratically on  $\mathbb{B}$ , this residual sign ambiguity is immaterial.

(ii) The multiplicative renormalization is carried out by introducing the SDE for the three-gluon vertex, which depends on the renormalization constant  $Z_3$ . It turns out that, by virtue of a massive cancellation triggered by the form of the BSE in (i), the multiplicative renormalization of the mass equation may be carried out exactly. The resulting manifestly finite expression is proportional to the parameter  $\omega$ . Thus, rather remarkably, in the absence of the non-cubic term in the BSE, the finite gluon mass vanishes, even in the presence of a non-vanishing  $\mathbb{B}(r)$ . Instead, when  $\omega$  assumes its natural value dictated by the BSE, the resulting gluon mass is non-vanishing; its value can be made compatible with the  $\Delta^{-1}(0)$  obtained from lattice simulations by adjusting the kernel of the BSE.

(iii) It turns out that the extensive cancellations mentioned in (ii) can be attributed to a concrete mathematical reason, namely the Fredholm alternatives theorem [96, 97], which is in full operation when  $\omega = 0$ . In that case, the kernels of the homogeneous BSE for  $\mathbb{B}(r)$

and of the inhomogeneous SDE for the three-gluon vertex are identical. Then, according to the theorem, no simultaneous solutions exist to these two integral equations unless a certain integral expression vanishes; and, quite notably, this expression is none other than the mass equation derived from the gluon SDE. Instead, the presence of a non-vanishing  $\omega$  introduces a difference between the two kernels, thus evading the main assumption of the theorem and leading to the emergence of a gluon mass.

The article is organized as follows. In Sec. II we review the theoretical framework employed in this work, focusing on the set of special relations pertaining to the SM. Then, certain key results are derived in Sec. III, which are extensively used in the ensuing analysis. In Sec. IV the renormalization of the relevant quantities is outlined, placing particular emphasis on the treatment of the components emerging from the activation of the SM. In Sec. V we derive in detail the BSE that controls the formation of the bound state pole, paying special attention to the novel term that causes the non-linearity of the resulting integral equation. In Sec. VI we explain in detail how the BSE of the previous section leads to the fixing of the scale of the solutions obtained. Then, in Sec. VII we carry out the multiplicative renormalization of the gluon mass, which proceeds through the implementation of a crucial cancellation. In Sec. VIII we state the Fredholm alternatives theorem, and apply it to the set of integral equations considered in the previous section. In Sec. IX we perform a detailed numerical analysis of the above equations, and study the dependence of the gluon mass and the displacement function on the details of the BSE kernel. In Sec. X we discuss our results and summarize our conclusions. Finally, in Appendix A we illustrate the central mathematical construction of Sec. VII by means of a concrete example.

## II. GENERAL THEORETICAL FRAMEWORK

In this section we introduce the necessary notation, and present a brief overview of the main notions associated with the implementation of the SM in the context of Yang-Mills theories; for recent reviews on the subject, see [51, 53].

Let us consider the (Landau-gauge) gluon propagator

$$\Delta_{\mu\nu}^{ab}(q) = -i\delta^{ab}P_{\mu\nu}(q)\Delta(q), \quad P_{\mu\nu}(q) := g_{\mu\nu} - q_\mu q_\nu/q^2, \quad (2.1)$$

and the associated dimensionless vacuum polarization  $\mathbf{\Pi}(q)$ ,

$$\Delta^{-1}(q) = q^2[1 + i\mathbf{\Pi}(q)]. \quad (2.2)$$

In addition, the three-gluon vertex,  $\mathcal{G}_{\alpha\mu\nu}^{abc}(q, r, p)$ , with all momenta incoming and  $q+r+p=0$ , is defined as

$$\mathcal{G}_{\alpha\mu\nu}^{abc}(q, r, p) = \langle 0|T[\tilde{A}_\alpha^a(q)\tilde{A}_\mu^b(r)\tilde{A}_\nu^c(p)]|0\rangle, \quad (2.3)$$

where  $\tilde{A}_\alpha^a$  denotes the Fourier transformed SU(3) gauge field, and  $T$  the standard time-ordering operation. It is convenient for the analysis that follows to explicitly factor out of  $\mathcal{G}_{\alpha\mu\nu}^{abc}(q, r, p)$  the gauge coupling  $g$ , thus defining the vertex  $\mathbb{\Gamma}_{\alpha\mu\nu}^{abc}(q, r, p)$ , according to

$$\begin{aligned} \mathcal{G}_{\alpha\mu\nu}^{abc}(q, r, p) &= g\mathbb{\Gamma}_{\alpha\mu\nu}^{abc}(q, r, p), \\ \mathbb{\Gamma}_{\alpha\mu\nu}^{abc}(q, r, p) &= f^{abc}\mathbb{\Gamma}_{\alpha\mu\nu}(q, r, p), \end{aligned} \quad (2.4)$$

where  $f^{abc}$  denotes the structure constants of the group SU(3).

Note that both  $\mathcal{G}_{\alpha\mu\nu}^{abc}(q, r, p)$  and  $\mathbb{\Gamma}_{\alpha\mu\nu}^{abc}(q, r, p)$  will be employed throughout this work; therefore, a clear diagrammatic distinction between them has been introduced in Fig. 1. At tree level,

$$\mathbb{\Gamma}_0^{\alpha\mu\nu}(q, r, p) = (q-r)^\nu g^{\alpha\mu} + (r-p)^\alpha g^{\mu\nu} + (p-q)^\mu g^{\nu\alpha}. \quad (2.5)$$

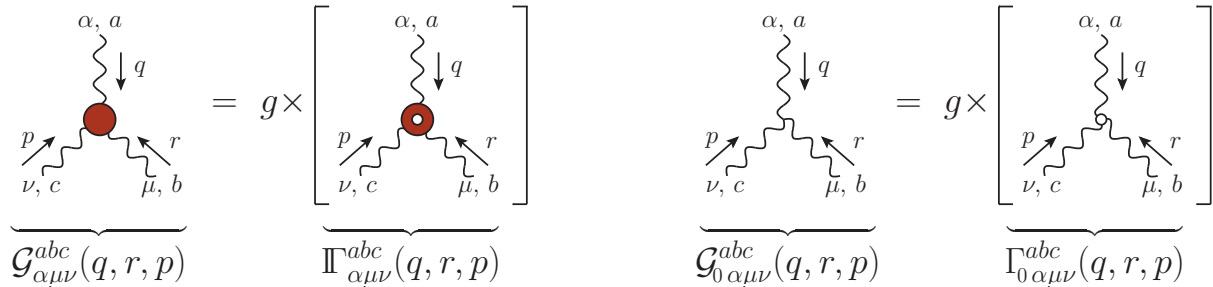


Figure 1. Diagrammatic conventions for the fully dressed three-gluon vertex (left) and its tree-level counterpart (right).

The cornerstone of the SM is the observation that if the function  $\mathbf{\Pi}(q)$  develops a pole at  $q^2 = 0$  (“massless pole”), then, in that kinematic limit, the propagator of the gauge boson saturates at a non-zero value [12, 13], according to the sequence (Euclidean space)

$$\lim_{q^2 \rightarrow 0} \mathbf{\Pi}(q) = m^2/q^2 \implies \lim_{q^2 \rightarrow 0} \Delta^{-1}(q) = \lim_{q^2 \rightarrow 0} (q^2 + m^2) \implies \Delta^{-1}(0) = m^2. \quad (2.6)$$

This effect is interpreted as the dynamical generation of a mass, which is identified with the positive residue of the pole.

In the absence of elementary scalar fields, massless poles may arise due to a variety of reasons [98–101]. In Yang-Mills theories, the pole formation proceeds through the fusion of two gluons or of a ghost-antighost pair into a *color-carrying* scalar bound state of vanishing mass [11, 14, 15, 49, 54–59], to be denoted by  $\Phi^a$ . In the case of the gluon fusion that we will consider throughout this work, the formation of this bound state is controlled by a special BSE; details of the solutions obtained are given in the following sections.

There are three main structures associated with this nonperturbative process, which are diagrammatically depicted in Fig. 2:

(i) The effective vertex describing the interaction between  $\Phi^a$  and two gluons, denoted by

$$B_{\mu\nu}^{abc}(q, r, p) = i f^{abc} B_{\mu\nu}(q, r, p). \quad (2.7)$$

(ii) The propagator of the massless composite scalar, denoted by

$$D_{\Phi}^{ab}(q) = \frac{i\delta^{ab}}{q^2}. \quad (2.8)$$

(iii) The transition amplitude,  $I_{\alpha}^{ab}(q) = \delta^{ab} I_{\alpha}(q)$ , connecting a gluon  $A_{\alpha}^a$  with a scalar  $\Phi^b$ ; Lorentz invariance imposes that

$$I_{\alpha}(q) = q_{\alpha} I(q), \quad (2.9)$$

where  $I(q)$  is a scalar form factor.

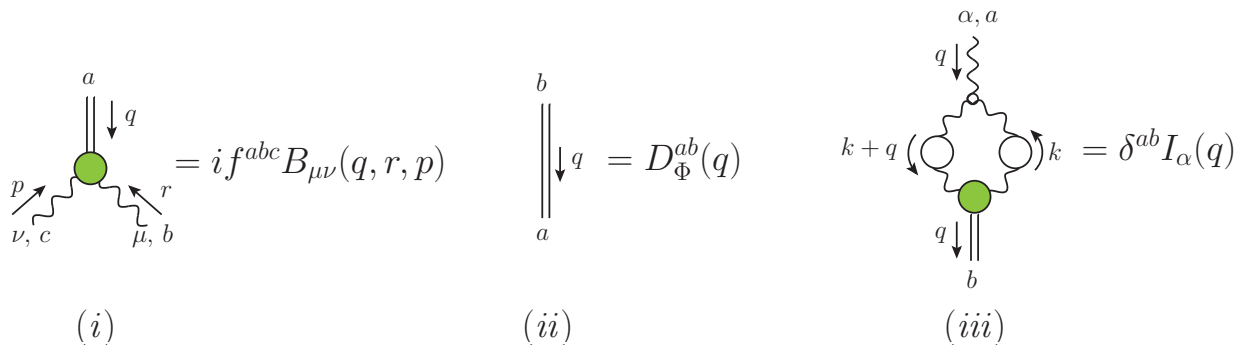


Figure 2. Left: The effective vertex  $B_{\mu\nu}^{abc}(q, r, p)$ , with Lorentz, color, and momentum conventions indicated. Center: The propagator of the massless composite scalar,  $D_{\Phi}^{ab}(q)$ . Right: Gluon-scalar transition amplitude,  $I_{\alpha}^{ab}(q)$ .

The emergence of items (i)-(iii) modifies profoundly the structure of the four-gluon kernel,  $\mathcal{T}_{\rho\sigma\mu\nu}^{mabc}(p_1, p_2, p_3, p_4)$ , entering in the skeleton expansion of the three-gluon vertex SDE, see Fig. 4. In particular, as shown diagrammatically in Fig. 3, we have that

$$\mathcal{T}_{\rho\sigma\mu\nu}^{mabc}(p_1, p_2, p_3, p_4) = \mathcal{K}_{\rho\sigma\mu\nu}^{mabc}(p_1, p_2, p_3, p_4) + \mathcal{M}_{\rho\sigma\mu\nu}^{mabc}(p_1, p_2, p_3, p_4), \quad (2.10)$$

where  $\mathcal{K}$  denotes the regular, pole-free term, while  $\mathcal{M}^{mabc}$  is given by

$$\mathcal{M}_{\rho\sigma\mu\nu}^{mabc}(p_1, p_2, p_3, p_4) = B_{\rho\sigma}^{mnx}(p_1, p_2, q) D_{\Phi}^{xe}(q) B_{\mu\nu}^{ebc}(p_3, p_4, -q), \quad (2.11)$$

with  $q = p_1 + p_2 = -p_3 - p_4$ .

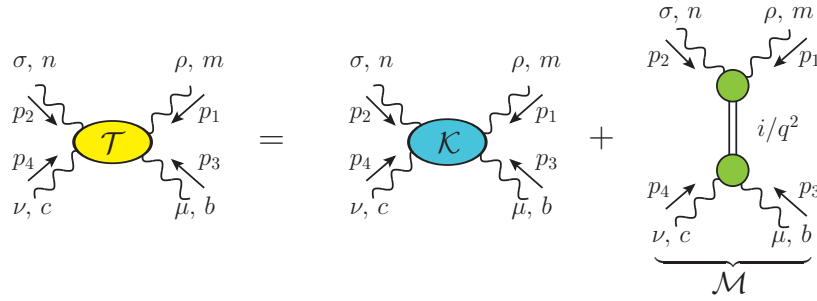


Figure 3. Decomposition of the four-gluon scattering kernel,  $\mathcal{T}_{\rho\sigma\mu\nu}^{mabc}(p_1, p_2, p_3, p_4)$ , into a regular part,  $\mathcal{K}_{\rho\sigma\mu\nu}^{mabc}(p_1, p_2, p_3, p_4)$ , and a massless pole part,  $\mathcal{M}_{\rho\sigma\mu\nu}^{mabc}(p_1, p_2, p_3, p_4)$ , according to Eq. (2.10).

We emphasize that, despite appearances, the kernel  $\mathcal{T}$  is one-particle irreducible, because the propagator  $D_{\Phi}(q)$ , present in the term  $\mathcal{M}$ , does not correspond to a fundamental field, but rather to a composite excitation, representing a multitude of gluon interactions.

The way how the pole in  $\mathcal{M}$  causes the saturation of the gluon propagator is through the three-gluon vertex. In particular, consider the SDE for the three-gluon vertex, whose diagrammatic representation is given in Fig. 4; note that only the diagrams relevant to our purposes are shown (first row). The insertion of  $\mathcal{M}^{mabc}$  in this SDE generates a new term for the three-gluon vertex (second row), to be denoted by  $V_{\alpha\mu\nu}(q, r, p)$ . Specifically,  $\mathbb{\Gamma}_{\alpha\mu\nu}(q, r, p)$  assumes the general form<sup>1</sup>

$$\mathbb{\Gamma}_{\alpha\mu\nu}(q, r, p) = \Gamma_{\alpha\mu\nu}(q, r, p) + V_{\alpha\mu\nu}(q, r, p), \quad (2.12)$$

<sup>1</sup> Due to the Bose symmetry of  $\mathbb{\Gamma}_{\alpha\mu\nu}(q, r, p)$ , poles appear also in the channels carrying momenta  $r$  or  $p$ , and are proportional to  $I_{\mu}(r)$  or  $I_{\nu}(p)$ . However, when these legs are internal to Feynman diagrams, they get annihilated due to the contraction with the corresponding Landau-gauge propagators.

where  $\Gamma_{\alpha\mu\nu}(q, r, p)$  represents the pole-free component, while  $V_{\alpha\mu\nu}(q, r, p)$  is given by

$$V_{\alpha\mu\nu}(q, r, p) = I_\alpha(q) \left( \frac{i}{q^2} \right) iB_{\mu\nu}(q, r, p), \quad (2.13)$$

as may be read off from Fig. 4. Then, due to Eq. (2.9), the term  $V_{\alpha\mu\nu}(q, r, p)$  becomes

$$V_{\alpha\mu\nu}(q, r, p) = - \left( \frac{q_\alpha}{q^2} \right) I(q) B_{\mu\nu}(q, r, p). \quad (2.14)$$

Evidently,  $V_{\alpha\mu\nu}(q, r, p)$  satisfies  $P^{\alpha'\alpha}(q)V_{\alpha\mu\nu}(q, r, p) = 0$ ; in that sense, the poles are said to be “*longitudinally coupled*”.

Now, since the SDE controlling the momentum evolution of the gluon propagator depends on the vertex  $\Gamma_{\alpha\mu\nu}(q, r, p)$ , the component  $V_{\alpha\mu\nu}(q, r, p)$  provides the massless pole required for the activation of the SM. Specifically, focusing on the part of the gluon propagator proportional to  $q_\mu q_\nu$ , we obtain the characteristic diagram shown in Fig. 5, composed by the “square” of the transition amplitude  $I_\alpha(q)$ . In particular, in the limit  $q \rightarrow 0$ , we have the central result [55–57]

$$m^2 = g^2 I^2, \quad (2.15)$$

where we have defined the short-hand notation  $I := I(0)$ .

Let us finally emphasize that, in order to elucidate the novel aspects of the method, in Figs. 4 and 5 we have omitted all diagrams containing ghosts as internal lines or four-gluon vertices. This omission poses no problem for the following two reasons. First, the omitted graphs do not interfere in any way with the results derived in what follows; for a brief discussion, see Sec. X. Second, we do not rely on the vertex SDE for an accurate description of the form factor  $L_{sg}$  [see Eq. (3.20)], appearing in some of the central formulas; instead, we use the available lattice results for this quantity [102–110].

### III. SETTING THE STAGE: KEY RESULTS AND MAIN PROPERTIES

In this section we present a collection of relations and properties that serve as prerequisites for deriving the main results of this work. Note that, while several of these items have already appeared in the literature, here we focus on aspects that are especially pertinent for the task at hand.



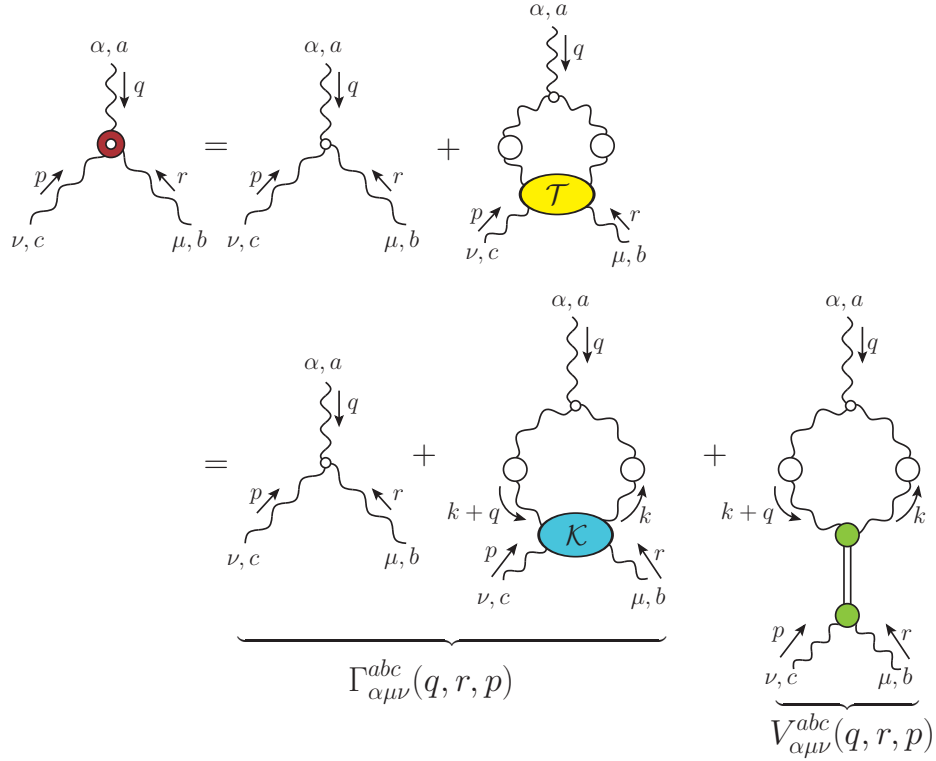


Figure 4. *First line:* SDE for the three-gluon vertex. *Second line:* The pole induced to the three-gluon vertex due to the  $\mathcal{M}$  component of  $\mathcal{T}$  in Eq. (2.10) (see also Fig. 3).

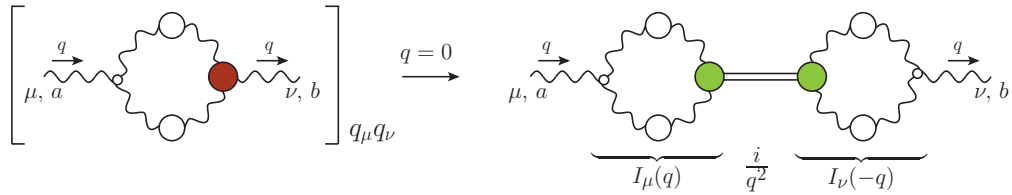


Figure 5. Relation between the gluon mass and the transition amplitude,  $I_{\alpha}(q)$ .

### A. An important limit

The kinematic limit relevant for the gluon mass generation is that of vanishing momentum transfer, or, in terms of the propagator diagram in Fig. 5, the limit  $q \rightarrow 0$ . It is therefore important to determine the behavior of the effective vertex  $B_{\mu\nu}(q, r, p)$  in that limit.

The general tensorial decomposition of this vertex is given by

$$B_{\mu\nu}(q, r, p) = B_1 g_{\mu\nu} + B_2 r_{\mu} r_{\nu} + B_3 p_{\mu} p_{\nu} + B_4 r_{\mu} p_{\nu} + B_5 p_{\mu} r_{\nu}, \quad (3.1)$$

and  $B_i := B_i(q, r, p)$ . The Bose symmetry of the full vertex  $B_{\mu\nu}^{abc}(q, r, p)$  under the exchange

of the two incoming gluons imposes that  $B_{\mu\nu}^{abc}(q, r, p) = B_{\nu\mu}^{acb}(q, p, r)$ , from which follows that  $B_{\mu\nu}(q, r, p) = -B_{\nu\mu}(q, p, r)$ . Then, setting in this last relation  $q = 0$  ( $p = -r$ ), we obtain  $B_{\mu\nu}(0, r, -r) = -B_{\nu\mu}(0, r, -r)$ . Given that

$$B_{\mu\nu}(0, r, -r) = B_1(0, r, -r) g_{\mu\nu} + C_1(0, r, -r) r_\mu r_\nu, \quad (3.2)$$

where  $C_1 := B_2 + B_3 - B_4 - B_5$ , we conclude immediately that

$$B_1(0, r, -r) = 0 = C_1(0, r, -r) \implies B_{\mu\nu}(0, r, -r) = 0. \quad (3.3)$$

Let us then consider the Taylor expansion of  $B_{\mu\nu}(q, r, p)$  around  $q = 0$ ,

$$B_{\mu\nu}(0, r, -r) = q^\alpha \mathcal{B}_{\alpha\mu\nu}(0, r, -r) + \dots, \quad (3.4)$$

where we have introduced the shorthand notation

$$\mathcal{B}_{\alpha\mu\nu}(0, r, -r) := \left[ \frac{\partial}{\partial q^\alpha} B^{\mu\nu}(q, r, -r - q) \right]_{q=0}, \quad (3.5)$$

accompanied by the diagrammatic representation shown in Fig. 6, and the ellipsis denotes terms of higher order in  $q$ . When taking the limit indicated in Eq. (3.5) we consider  $r$  to be independent of  $q$ , in which case, due to conservation of four-momentum,  $p$  depends on  $q$ , since  $p = -q - r$ ; therefore,  $\partial p^\mu / \partial q^\alpha = -g_\alpha^\mu$ .

The next step is to contract  $\mathcal{B}_{\alpha\mu\nu}(0, r, -r)$  by  $P_{\mu'}^\mu(r) P_{\nu'}^\nu(r)$ ; this contraction appears naturally in the diagrams where  $B_{\mu\nu}(q, r, p)$  is inserted, because the two gluon propagators attached to it are in the Landau gauge. Then, since the tensorial decomposition of  $\mathcal{B}_{\alpha\mu\nu}(0, r, -r)$  is given by

$$\mathcal{B}_{\alpha\mu\nu}(0, r, -r) = \mathcal{B}_1(r) r_\alpha g_{\mu\nu} + \mathcal{B}_2(r) [r_\alpha g_{\mu\nu} + r_\mu g_{\alpha\nu} + r_\nu g_{\mu\alpha}] + \mathcal{B}_3(r) r_\alpha r_\mu r_\nu, \quad (3.6)$$

only the first term survives this contraction, *i.e.*,

$$\mathcal{B}_{\alpha\mu\nu}(0, r, -r) P_{\mu'}^\mu(r) P_{\nu'}^\nu(r) = \mathcal{B}_1(r) r_\alpha P_{\mu'\nu'}(r). \quad (3.7)$$

It is now straightforward to establish that

$$r_\alpha \mathcal{B}_1(r) = \left[ \frac{\partial}{\partial q^\alpha} B_1(q, r, -r - q) \right]_{q=0} = 2r_\alpha \underbrace{\left[ \frac{\partial B_1(q, r, p)}{\partial p^2} \right]_{q=0}}_{\mathbb{B}(r)}, \quad (3.8)$$

or

$$\mathcal{B}_1(r) = 2\mathbb{B}(r), \quad (3.9)$$

from which follows that

$$\mathcal{B}_{\alpha\mu\nu}(0, r, -r) = 2\mathbb{B}(r) r_\alpha g_{\mu\nu} + \dots, \quad (3.10)$$

and then, from Eq. (3.4),

$$B_{\mu\nu}(0, r, -r) = 2(q \cdot r) \mathbb{B}(r) g_{\mu\nu} + \dots, \quad (3.11)$$

where the ellipses denote terms that get annihilated upon the aforementioned contraction. The diagrammatic representation of Eq. (3.10) is shown in Fig. 6, and will be used in the analysis that follows.

Figure 6. Diagrammatic representation of Eq. (3.10), corresponding to the first nonvanishing term in the Taylor expansion of  $B_{\mu\nu}^{abc}(q, r, p)$  around  $q = 0$ .

## B. The gluon-scalar transition amplitude

Given the central relation of Eq. (2.15), we next derive a convenient expression that allows us to compute the form factor  $I$  in terms of the basic quantities entering in its diagrammatic definition, see Fig. 2, item (iii).

For general momentum  $q$ , the transition amplitude  $I^\alpha(q)$  is given by

$$I^\alpha(q) = -\frac{iC_A}{2} \int_k \Gamma_0^{\alpha\beta\lambda}(q, k, -k - q) \Delta_{\beta\mu}(k) \Delta_{\lambda\nu}(k + q) B^{\mu\nu}(-q, -k, k + q), \quad (3.12)$$

where Eq. (2.7) was employed, the symmetry factor  $\frac{1}{2}$  has been supplied, and  $C_A$  is the Casimir eigenvalue of the adjoint representation [ $N$  for  $SU(N)$ ]. In addition, we use the shorthand notation

$$\int_k := \frac{1}{(2\pi)^4} \int d^4k, \quad (3.13)$$

where the use of a symmetry-preserving regularization scheme is implicitly assumed.

Then, by virtue of Eq. (2.9), it is elementary to establish that

$$I = \frac{1}{4} \left[ \frac{\partial I^\alpha(q)}{\partial q^\alpha} \right]_{q=0}. \quad (3.14)$$

So, from Eq. (3.12) we obtain

$$4I = -\frac{iC_A}{2} \int_k \left[ \frac{\partial}{\partial q^\alpha} \Gamma_0^{\alpha\beta\lambda}(q, k, -k-q) \Delta_{\beta\mu}(k) \Delta_{\lambda\nu}(k+q) \right]_{q=0} B^{\mu\nu}(0, -k, k) \\ - \frac{iC_A}{2} \int_k \Gamma_0^{\alpha\beta\lambda}(0, k, -k) \Delta_\beta^\mu(k) \Delta_\lambda^\nu(k) \mathcal{B}_{\alpha\mu\nu}(0, -k, k), \quad (3.15)$$

and since  $B_{\mu\nu}(0, -k, k) = 0$  [see Eq. (3.3)], we have

$$4I = -\frac{iC_A}{2} \int_k \Gamma_0^{\alpha\beta\lambda}(0, k, -k) \Delta_\beta^\mu(k) \Delta_\lambda^\nu(k) \mathcal{B}_{\alpha\mu\nu}(0, -k, k). \quad (3.16)$$

To further evaluate Eq. (3.15), use Eq. (2.5) to get

$$\Gamma_0^{\alpha\beta\lambda}(0, k, -k) = 2k^\alpha g^{\beta\lambda} - k^\lambda g^{\alpha\beta} - k^\beta g^{\alpha\lambda}, \quad (3.17)$$

and then Eq. (3.10) (with  $r \rightarrow -k$ ), to finally obtain

$$I = -\frac{3iC_A}{2} \int_k k^2 \Delta^2(k) \mathbb{B}(k). \quad (3.18)$$

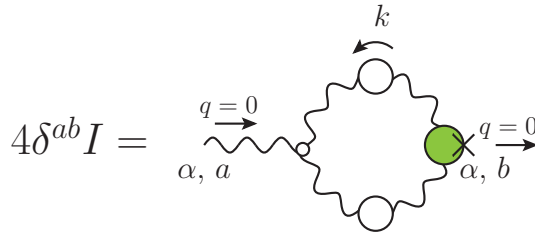


Figure 7. Diagrammatic definition of the scalar form factor,  $I$ , of the transition amplitude.

### C. SDE of the three-gluon vertex and its soft gluon limit

The soft-gluon limit of the SDE for  $\Gamma_{\alpha\mu\nu}^{abc}(q, r, p)$  is of central importance for the ensuing analysis; indeed, as will be shown in detail in Sec. VII, its proper use leads to considerable simplifications at the level of the mass equation. In order to elucidate this important aspect,

we employ a simplified version of the SDE, which contains precisely the structure required for certain crucial relations to be triggered. Specifically, we consider the SDE represented in Fig. 8, composed only by the tree-level contribution ( $a_1$ ) and the diagram ( $a_2$ ), while diagrams where the gluon with momentum  $q$  couples to a ghost-gluon or a four-gluon vertex are omitted<sup>2</sup>. The reason why diagram ( $a_2$ ) is singled out is because its kernel  $\mathcal{K}$  appears also in the BSE for  $\mathbb{B}(r)$ , shown in Fig. 10. This, in turn, will be instrumental for the implementation of the renormalization procedure outlined in Sec. VII

Note that, in the standard version of this SDE, the three-gluon vertex in diagram ( $a_2$ ) is kept at tree level. The form employed here, with the three-gluon vertex fully-dressed, corresponds to the BSE analogue of this equation [111–116]. Consequently, the skeleton expansion of the kernel  $\mathcal{K}$ , given in Fig. 9, does not contain certain classes of diagrams (*e.g.*, ladder graphs) in order to avoid overcounting. In fact, ghost loops aside, the diagrams of Fig. 9 comprise precisely the kernel of the standard glueball BSE [117, 118]. The main advantage of this version of the SDE is that the additional fully-dressed vertex absorbs the vertex renormalization  $Z_3$ , defined in Eq. (4.1), which otherwise would be multiplying the tree-level vertex; as a result, renormalization may be carried out subtractively rather than multiplicatively. In particular, the validity of the special formula in Eq. (4.18) hinges precisely on graph ( $a_2$ ) having a fully-dressed three-gluon vertex.

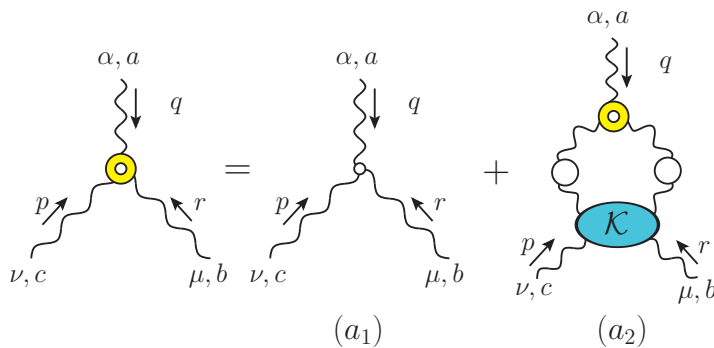


Figure 8. SDE for the regular part of the three-gluon vertex,  $\Gamma_{\alpha\mu\nu}^{abc}(q, r, p)$ , in BS form.

We next factor out the color structure  $f^{abc}$  by setting  $\Gamma_{\alpha\mu\nu}^{abc}(q, r, p) = f^{abc}\Gamma_{\alpha\mu\nu}(q, r, p)$ , and focus on the soft gluon limit,  $\Gamma_{\alpha\mu\nu}(0, r, -r)$ . The reason for this choice is that, eventually, this vertex will be used in the graph of Eq. (5), which is evaluated precisely in this kinematic

<sup>2</sup> The role of these terms will be discussed in section Sec. X.

limit. Setting  $q = 0$  into Fig. 8, we get

$$\Gamma_{\alpha\mu\nu}^{abc}(0, r, -r) = \Gamma_{0\alpha\mu\nu}^{abc}(0, r, -r) + \int_k \Gamma_{\alpha\gamma\delta}^{axe}(0, k, -k) \Delta_{xm}^{\gamma\rho}(k) \Delta_{en}^{\delta\sigma}(k) \mathcal{K}_{\rho\sigma\mu\nu}^{mabc}(-k, k, r, -r). \quad (3.19)$$

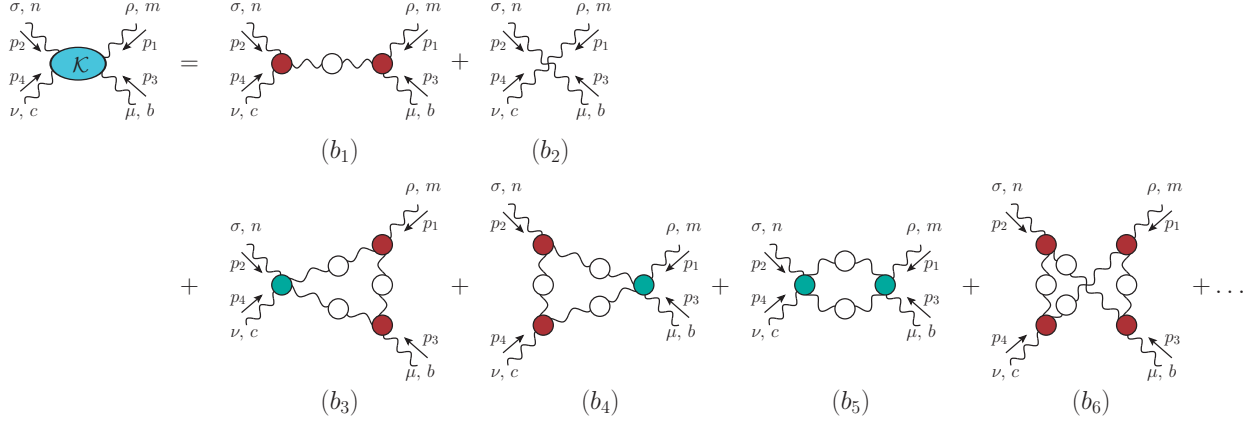


Figure 9. Skeleton expansion of the scattering kernel,  $\mathcal{K}_{\rho\sigma\mu\nu}^{mabc}(p_1, p_2, p_3, p_4)$ . The one-gluon exchange is highlighted and the ellipsis denotes contributions with two or more loops.

To proceed further, consider the contraction of  $\Gamma_{\alpha\mu\nu}(0, r, -r)$  by  $P_{\mu'}^{\mu}(r)P_{\nu'}^{\nu}(r)$ ; it is elementary to establish that this vertex projection is described by a single form factor, denoted by  $L_{sg}(r)$ , namely [59, 106]

$$P_{\mu'}^{\mu}(r)P_{\nu'}^{\nu}(r)\Gamma_{\alpha\mu\nu}(0, r, -r) = 2L_{sg}(r)r_{\alpha}P_{\mu'\nu'}(r). \quad (3.20)$$

Note that, in the Landau gauge that we employ, the  $\Gamma_{\alpha\gamma\delta}^{axe}(0, k, -k)$  on the r.h.s. of Eq. (3.19) is automatically contracted by two transverse projectors, thus triggering Eq. (3.20) therein. Then, contracting both sides of Eq. (3.19) by  $P_{\mu'}^{\mu}(r)P_{\nu'}^{\nu}(r)$ , we obtain

$$\begin{aligned} f^{abc}L_{sg}(r)r_{\alpha}P_{\mu'\nu'}(r) &= f^{abc}r_{\alpha}P_{\mu'\nu'}(r) \\ &\quad - f^{amn} \int_k k_{\alpha}L_{sg}(k)\Delta^2(k)P^{\rho\sigma}(k)\mathcal{K}_{\rho\sigma\mu\nu}^{mabc}(-k, k, r, -r)P_{\mu'}^{\mu}(r)P_{\nu'}^{\nu}(r). \end{aligned} \quad (3.21)$$

Lastly, we contract Eq. (3.21) with  $f^{abc}r^{\alpha}g^{\mu'\nu'}$  to eliminate the color and Lorentz indices. Using that  $P_{\mu}^{\mu}(r) = 3$ , and that for  $SU(N)$ ,  $f^{abc}f^{abc} = C_A(N^2 - 1)$ , we obtain

$$L_{sg}(r) = 1 + \alpha_s \int_k k^2 \Delta^2(k) K(r, k) L_{sg}(k), \quad (3.22)$$

with the kernel  $K(r, k)$  defined as

$$\alpha_s K(r, k) := -\frac{(r \cdot k)}{c r^2 k^2} f^{abc} f^{amn} P^{\mu\nu}(r) P^{\rho\sigma}(k) \mathcal{K}_{\rho\sigma\mu\nu}^{mabc}(-k, k, r, -r), \quad (3.23)$$

where we explicitly factor out the strong charge  $\alpha_s = g^2/4\pi$ . The numerical factor  $c := 3C_A(N^2 - 1)$  arises from the projections of Lorentz and color indices; for  $N = 3$ ,  $c = 72$ .

#### D. Displacement of the Ward identity of the three-gluon vertex

In addition to triggering the SM, the massless poles are crucial for preserving gauge invariance: their inclusion in the off-shell interaction vertices guarantees that the Slavnov-Taylor identities (STIs) [119, 120] of the theory retain the exact same form before and after mass generation [121]. In the case of the three-gluon vertex, the presence of these poles gives rise to a characteristic effect, namely the displacement of the WI satisfied by the soft-gluon form factor  $L_{sg}(r)$  [59, 76], introduced in Eq. (3.20).

In particular, let us denote by  $L_{sg}(r)$  and  $L_{sg}^*(r)$  the corresponding form factor when the SM is turned on and off, respectively. When the SM is off, the three-gluon vertex is simply given by  $\Gamma_{\alpha\mu\nu}(q, r, p)$ , and the STI it satisfies is given by [4, 122–124]

$$q^\alpha \Gamma_{\alpha\mu\nu}(q, r, p) \mathcal{T}_{\mu'\nu'}^{\mu\nu}(r, p) = F(q^2) [\Delta^{-1}(p^2) H_{\nu\mu}(p, q, r) - \Delta^{-1}(r^2) H_{\mu\nu}(r, q, p)] \mathcal{T}_{\mu'\nu'}^{\mu\nu}(r, p), \quad (3.24)$$

where  $\mathcal{T}_{\mu'\nu'}^{\mu\nu}(r, p) := P_{\mu'}^\mu(r) P_{\nu'}^\nu(p)$ ,  $F(q)$  denotes the ghost dressing function, defined from the ghost propagator,  $D^{ab}(q)$ , by  $D^{ab}(q) = i\delta^{ab} F(q)/q^2$ , and  $H_{\nu\mu}(p, q, r)$  is the ghost-gluon kernel.

Taking the limit  $q \rightarrow 0$  of both sides of Eq. (3.24), also known as the “soft-gluon limit”, one obtains the corresponding WI, which simply states that

$$L_{sg}^*(r^2) = [\text{r.h.s. of STI in Eq. (3.24)}]_{q \rightarrow 0}. \quad (3.25)$$

When the SM is activated, the vertex that satisfies the STI of Eq. (3.24) is the *full*  $\Gamma_{\alpha\mu\nu}(q, r, k)$ , given by Eq. (2.12). In particular, with the aid of Eq. (2.14), the l.h.s. of Eq. (3.24) becomes

$$q^\alpha \Gamma_{\alpha\mu\nu}(q, r, p) \mathcal{T}_{\mu'\nu'}^{\mu\nu}(r, p) = [q^\alpha \Gamma_{\alpha\mu\nu}(q, r, p) - I(q) B_{\mu\nu}(q, r, p)] \mathcal{T}_{\mu'\nu'}^{\mu\nu}(r, p), \quad (3.26)$$

while the r.h.s. remains exactly the same. Then, as has been shown in [59, 76], the limit  $q \rightarrow 0$  of the STI yields

$$L_{sg}(r^2) = L_{sg}^*(r^2) + \mathbb{C}(r^2), \quad (3.27)$$

where

$$\mathbb{C}(r) := -I \mathbb{B}(r), \quad (3.28)$$

is denominated the “*displacement function*”.

The importance of this result is that one may determine  $\mathbb{C}(r)$  as the difference between the  $L_{sg}(r^2)$ , extracted directly from the lattice, and the expression for  $L_{sg}^*(r^2)$  on the r.h.s. of Eq. (3.25), which is evaluated using lattice inputs for its various components [59, 76]. The result for  $\mathbb{C}(r)$  that emerges through this procedure will serve as benchmark for the numerical analysis presented in Sec. IX.

#### IV. RENORMALIZATION: GENERAL CONSIDERATIONS

In this section we discuss in detail the renormalization of the key dynamical components that emerge from the activation of the SM. In particular, we will focus on the renormalization properties of the central quantities  $I$  and  $B_{\mu\nu}$ .

We focus exclusively on the gluon propagator and the three-gluon vertex, which are the two basic ingredients comprising the structures considered in this work. Denoting by the index “R” the renormalized quantities, we have

$$\Delta_R(q^2) = Z_A^{-1} \Delta(q^2), \quad \mathbb{I}_R^{\alpha\mu\nu}(q, r, p) = Z_3 \mathbb{I}^{\alpha\mu\nu}(q, r, p), \quad g_R = Z_g^{-1} g, \quad (4.1)$$

where  $Z_A^{1/2}$  is the wave function renormalization constants of the gluon field,  $Z_3$  the renormalization constant of the three-gluon vertex, and  $Z_g$  the coupling renormalization constant, given by

$$Z_g = Z_3 Z_A^{-3/2}. \quad (4.2)$$

Furthermore, we will introduce two additional renormalization constants, to be denoted by  $Z_I$  and  $Z_B$ , which renormalize the quantities  $I$  and  $B^{\mu\nu}(q, r, p)$ , respectively, according to [125]

$$I_R = Z_I^{-1} I, \quad B_R^{\mu\nu}(q, r, p) = Z_B^{-1} B^{\mu\nu}(q, r, p). \quad (4.3)$$

The partial derivatives of  $B^{\mu\nu}(q, r, p)$  also renormalize in the same way, namely

$$\mathcal{B}_R^{\alpha\mu\nu}(0, r, -r) = Z_B^{-1} \mathcal{B}_R^{\alpha\mu\nu}(0, r, -r), \quad \mathbb{B}_R(r) = Z_B^{-1} \mathbb{B}(r). \quad (4.4)$$

Given that both the  $I$  and  $B^{\mu\nu}$  are composed by the fundamental fields and vertices, it is natural to expect that the  $Z_I$  and  $Z_B$  should be expressed in terms of the  $Z_A$  and  $Z_3$



introduced in Eq. (4.1); indeed, we find that [125]

$$Z_I = Z_3^{-1} Z_A, \quad Z_B = Z_A^{-1}. \quad (4.5)$$

To see how the relations in Eq. (4.5) arise, we first turn to Eq. (2.15). Since  $m^2 := \Delta^{-1}(0)$ , from the first relation in Eq. (4.1) we have that [57, 125]

$$m^2 = Z_A^{-1} m_R^2. \quad (4.6)$$

On the other hand, combining Eq. (2.15), the first relation in Eq. (4.3), and Eq. (4.2), we have

$$m^2 = g^2 I^2 = Z_g^2 Z_I^2 \underbrace{g_R^2 I_R^2}_{m_R^2} = Z_3^2 Z_A^{-3} Z_I^2 m_R^2. \quad (4.7)$$

Then, the direct comparison of Eqs. (4.6) and (4.7) leads immediately to the first relation of Eq. (4.5).

The second relation in Eq. (4.5) may be obtained from Eq. (3.28), by noticing that, since  $V_{\alpha\mu\nu}(q, r, p)$  is a component of the three-gluon vertex  $\Pi^{\alpha\mu\nu}(q, r, p)$ , it is renormalized as in Eq. (4.1), namely

$$V^{\alpha\mu\nu}(q, r, p) = Z_3^{-1} V_R^{\alpha\mu\nu}(q, r, p), \quad (4.8)$$

and, therefore,

$$\mathbb{C}(k) = Z_3^{-1} \mathbb{C}_R(k). \quad (4.9)$$

On the other hand, from Eq. (3.28), using Eq. (4.3) and the first relation of Eq. (4.5), we have that

$$\mathbb{C}(k) = -Z_I Z_B \underbrace{I_R \mathbb{B}_R(k)}_{-\mathbb{C}_R(k)} = Z_3^{-1} Z_A Z_B \mathbb{C}_R(k). \quad (4.10)$$

Then, the comparison between Eqs. (4.9) and (4.10) yields the second relation of Eq. (4.5).

We next turn to the renormalization of the kernel  $\mathcal{K}_{\rho\sigma\mu\nu}^{mabc}(q, r, p, t)$ , appearing in Eq. (3.19), and later on in Eq. (5.4). To that end, notice that  $\mathcal{K}$  is a part of the four-gluon amplitude  $\mathcal{G}_{\rho\sigma\mu\nu}^{mabc}(q, r, p, t) = \langle 0 | T[\tilde{A}_\rho^m(q) \tilde{A}_\sigma^n(r) \tilde{A}_\mu^b(p) \tilde{A}_\nu^c(t)] | 0 \rangle$ , with the external legs amputated, *i.e.*,

$$\mathcal{G}(q, r, p, t) = \Delta(q)\Delta(r)\Delta(p)\Delta(t)\mathcal{K}(q, r, p, t) + \dots \quad (4.11)$$

where the ellipsis denotes the diagrams excluded when switching from the SDE to the BSE kernel, as discussed in Sec. III C. Since,  $A_R^{a\mu} = Z_A^{1/2} A^{a\mu}$ , the definition of  $\mathcal{G}$  in terms of gauge fields implies that  $\mathcal{G}_R = Z_A^{-2} \mathcal{G}$ . Therefore, from Eqs. (4.11) and (4.1), we get

$$\mathcal{K}_R(q, r, p, t) = Z_A^2 \mathcal{K}(q, r, p, t), \quad (4.12)$$

and, since  $\mathcal{K} \sim \alpha_s K$ , we have

$$K_R(q, r, p, t) = Z_A^2 Z_g^2 K(q, r, p, t). \quad (4.13)$$

From the above relations it is immediate to establish that the combinations  $\Delta\mathbb{B}$ ,  $\Delta^2\mathcal{K}$ , and  $\alpha_s\Delta^2K$  are renormalization-group invariant (RGI), *i.e.*,

$$\Delta\mathbb{B} = \Delta_R\mathbb{B}_R, \quad \Delta^2\mathcal{K} = \Delta_R^2\mathcal{K}_R, \quad \alpha_s\Delta^2K = \alpha_s^R\Delta_R^2K_R. \quad (4.14)$$

Note that, by virtue of the renormalization rule  $B_R^{\mu\nu} = Z_A B^{\mu\nu}$ , given by Eqs. (4.3) and (4.5), the kernel  $\mathcal{M}$  defined in Eq. (2.11) renormalizes as  $\mathcal{M}_R = Z_A^2 \mathcal{M}$ , *i.e.*, exactly as the kernel  $\mathcal{K}$  in Eq. (4.12); this is consistent with the fact that both  $\mathcal{K}$  and  $\mathcal{M}$  are parts of the same four-gluon kernel, see Eq. (2.10) and Fig. 4.

Armed with the above results, we may now derive a useful expression for the  $I_R$ , using Eq. (3.16) as our point of departure. Substituting the bare quantities comprising Eq. (3.16) by renormalized ones, we have

$$4Z_I I_R = -\frac{iC_A}{2} Z_A^2 Z_B \int_k \Gamma_0^{\alpha\beta\lambda}(0, k, -k) \Delta_{R\beta}^\mu(k) \Delta_{R\lambda}^\nu(k) \mathcal{B}_{R\alpha\mu\nu}(0, -k, k), \quad (4.15)$$

and, after employing Eq. (4.5),

$$4I_R = -\frac{iC_A}{2} Z_3 \int_k \Gamma_0^{\alpha\beta\lambda}(0, k, -k) \Delta_{R\beta}^\mu(k) \Delta_{R\lambda}^\nu(k) \mathcal{B}_{R\alpha\mu\nu}(0, -k, k), \quad (4.16)$$

or, from Eq. (3.18),

$$I_R = -\frac{3iC_A}{2} Z_3 \int_k k^2 \Delta_R^2(k) \mathbb{B}_R(k). \quad (4.17)$$

We finally turn to the renormalization of Eq. (3.22). By virtue of Eq. (3.20), it is clear that  $L_{sg}^R(r) = Z_3 L_{sg}(r)$ . Then, using Eq. (4.14), it is straightforward to show that the renormalized version of Eq. (3.22) is given by

$$L_{sg}^R(r) = Z_3 + \alpha_s^R \int_k k^2 \Delta_R^2(k) K_R(r, k) L_{sg}^R(k). \quad (4.18)$$

As announced in Sec. III C, the renormalization required for Eq. (4.18) is subtractive.

In what follows we will suppress the index ‘‘R’’ in order to avoid notational clutter.

## V. NON-LINEAR BETHE-SALPETER EQUATION FOR POLE FORMATION

In this section we derive the BSE satisfied by the amplitude  $\mathbb{B}(r)$ . This type of equation has been derived in the literature before [55–59]; however, in contradistinction to these earlier versions, the present BSE is not linearized, having its cubic nature fully retained.

The diagrammatic form of the BSE for general  $q$  is shown in the left part of Fig. 10, where the four-gluon kernel  $\mathcal{T}$  is depicted in Fig. 3. Specifically, from the first equality of Fig. 10 we have

$$B_{\mu\nu}^{abc}(q, r, p) = (G_{\mathcal{T}})_{\mu\nu}^{abc}(q, r, p), \quad (5.1)$$

where

$$(G_{\mathcal{T}})_{\mu\nu}^{abc}(q, r, p) = \int_k B_{\alpha\beta}^{axe}(q, k, -k - q) \Delta_{xm}^{\alpha\rho}(k) \Delta_{en}^{\beta\sigma}(k + q) \mathcal{T}_{\rho\sigma\mu\nu}^{mabc}(-k, k + q, r, p). \quad (5.2)$$

Then, after using Eqs. (2.10) and (2.11), two distinct terms arise, namely

$$(G_{\mathcal{T}})_{\mu\nu}^{abc}(q, r, p) = (G_{\mathcal{K}})_{\mu\nu}^{abc}(q, r, p) + (G_{\mathcal{M}})_{\mu\nu}^{abc}(q, r, p), \quad (5.3)$$

with

$$(G_{\mathcal{K}})_{\mu\nu}^{abc}(q, r, p) = \int_k B_{\alpha\beta}^{axe}(q, k, -k - q) \Delta_{xm}^{\alpha\rho}(k) \Delta_{en}^{\beta\sigma}(k + q) \mathcal{K}_{\rho\sigma\mu\nu}^{mabc}(-k, k + q, r, p),$$

$$(G_{\mathcal{M}})_{\mu\nu}^{abc}(q, r, p) = \Omega^{ad}(q) D_{\Phi}^{ds}(q) B_{\mu\nu}^{abc}(q, r, p), \quad (5.4)$$

where (symmetry factor  $\frac{1}{2}$  included)

$$\Omega^{ad}(q) = \frac{1}{2} \int_k B_{\alpha\beta}^{axe}(q, k, -k - q) \Delta_{xm}^{\alpha\rho}(k) \Delta_{en}^{\beta\sigma}(k + q) B_{\sigma\rho}^{dnm}(-q, k + q, -k). \quad (5.5)$$

Note that, while the term  $(G_{\mathcal{K}})$  is linear in  $B_{\mu\nu}^{abc}$ , the term  $(G_{\mathcal{M}})$  is cubic. As a result, the scale ambiguity of the solutions, present when only the term  $(G_{\mathcal{K}})$  is considered, is now eliminated (see next section).

Next, it is important to establish that the product  $\Omega^{ad}(q) D_{\Phi}^{ds}(q)$  appearing in  $(G_{\mathcal{M}})$  is finite as  $q \rightarrow 0$ ; this is so, because, in that limit,  $\Omega^{ad}(q) \sim q^2 \delta^{ad}$ , thus cancelling exactly the massless pole in  $D_{\Phi}^{ds}(q)$ .

To derive this key result from Eq. (5.5), set first  $\Omega^{ad}(q) = \delta^{ad} \Omega(q)$  and carry out the color algebra to obtain

$$\Omega(q) = \frac{C_A}{2} \int_k B_{\alpha\beta}(q, k, -k - q) P^{\alpha\rho}(k) P^{\beta\sigma}(k + q) B_{\rho\sigma}(-q, -k, k + q) \Delta(k) \Delta(k + q). \quad (5.6)$$

Then, taking the limit  $q \rightarrow 0$  of Eq. (5.6) using Eq. (3.11), we find

$$\begin{aligned} \lim_{q \rightarrow 0} \Omega(q) &= \frac{C_A}{2} \int_k B_{\alpha\beta}(0, k, -k) P^{\alpha\rho}(k) P^{\beta\sigma}(k) B_{\sigma\rho}(0, k, -k) \Delta^2(k) \\ &= 6C_A \int_k (q \cdot k)^2 \Delta^2(k) \mathbb{B}^2(k), \end{aligned} \quad (5.7)$$

and thus

$$\lim_{q \rightarrow 0} \Omega(q) = q^2 \tilde{\omega}, \quad \tilde{\omega} := \frac{3C_A}{2} \int_k k^2 \Delta^2(k) \mathbb{B}^2(k). \quad (5.8)$$

With this result in hand, it is immediate to establish that

$$(G\mathcal{M})_{\mu\nu}^{abc}(0, r, -r) = \omega B_{\mu\nu}^{abc}(0, r, -r), \quad \omega := i \tilde{\omega}; \quad (5.9)$$

therefore, this term combines directly with the term  $B_{\mu\nu}^{abc}(q, r, p)$  on the l.h.s of Eq. (5.1) in the same limit. In particular, after defining the new variable,

$$t := 1 - \omega, \quad (5.10)$$

Eq. (5.1) becomes

$$t B_{\mu\nu}^{abc}(0, r, -r) = \int_k B_{\alpha\beta}^{axe}(0, k, -k) \Delta_{xm}^{\alpha\rho}(k) \Delta_{en}^{\beta\sigma}(k) \mathcal{K}_{\rho\sigma\mu\nu}^{mabc}(-k, k, r, -r). \quad (5.11)$$

Given Eq. (3.3), it is clear that, in the limit  $q = 0$ , Eq. (5.11) yields to lowest order a trivial result ( $0 = 0$ ). So, in order to extract nontrivial information from it, one must equate the terms linear in  $q$  on both of its sides. Specifically, using Eq. (3.4) for the  $B_{\mu\nu}(0, r - r)$  and  $B_{\alpha\beta}(0, k - k)$  appearing in Eq. (5.11), one obtains the equation<sup>3</sup>

$$\mathcal{B}_{\lambda\mu\nu}^{abc}(0, r, -r) = t^{-1} \int_k \mathcal{B}_{\lambda\alpha\beta}^{axe}(0, k, -k) \Delta_{xm}^{\alpha\rho}(k) \Delta_{en}^{\beta\sigma}(k) \mathcal{K}_{\rho\sigma\mu\nu}^{mabc}(-k, k, r, -r), \quad (5.12)$$

which admits the diagrammatic representation given in the second line of Fig. 10.

Then, contracting both sides by  $P_{\mu'}^\mu(r) P_{\nu'}^\nu(r)$  and employing Eq. (3.7), we get

$$f^{abc} \mathbb{B}(r) r_\lambda P_{\mu'\nu'}(r) = -t^{-1} f^{amn} \int_k \mathbb{B}(k) \Delta^2(k) k_\lambda P^{\sigma\rho}(k) \mathcal{K}_{\rho\sigma\mu\nu}^{mabc}(-k, k, r, -r) P_{\mu'}^\mu(r) P_{\nu'}^\nu(r), \quad (5.13)$$

and, after contracting both sides by  $f^{abc} r^\lambda g^{\mu'\nu'}$ , and using that  $P_\mu^\mu(r) = 3$ , we arrive at the following equation for the amplitude  $\mathbb{B}(r)$ ,

$$\mathbb{B}(r) = t^{-1} \alpha_s \int_k k^2 \Delta^2(k) K(r, k) \mathbb{B}(k), \quad (5.14)$$

where  $K(r, k)$  is *exactly* the kernel defined in Eq. (3.23).

We end this section by pointing out that Eq. (5.14) is RGI. This follows directly by observing that, due to the first relation in Eq. (4.14),  $\tilde{\omega}$  itself, defined through Eq. (5.8), is

---

<sup>3</sup> We assume that  $t \neq 0$ ; if  $t = 0$ , the l.h.s. of Eq. (5.11) vanishes, and the resulting equation is no longer of the BSE type.

RGI, and so is the  $t$  in Eq. (5.10) *i.e.*,  $\omega = \omega_R$  and  $t = t_R$ . Then, the full BSE in Eq. (5.14) is RGI due to the third relation in Eq. (4.14), and the fact that the  $Z_B$  introduced to renormalize the  $\mathbb{B}$  cancels on both sides. As a result, one may substitute into Eq. (5.14) directly bare for renormalized quantities, without any renormalization constants appearing in the final expression, *i.e.*,

$$\mathbb{B}_R(r) = t_R^{-1} \alpha_s^R \int_k k^2 \Delta_R^2(k) K_R(r, k) \mathbb{B}_R(k). \quad (5.15)$$

Again, the index ‘‘R’’ will be suppressed in what follows.

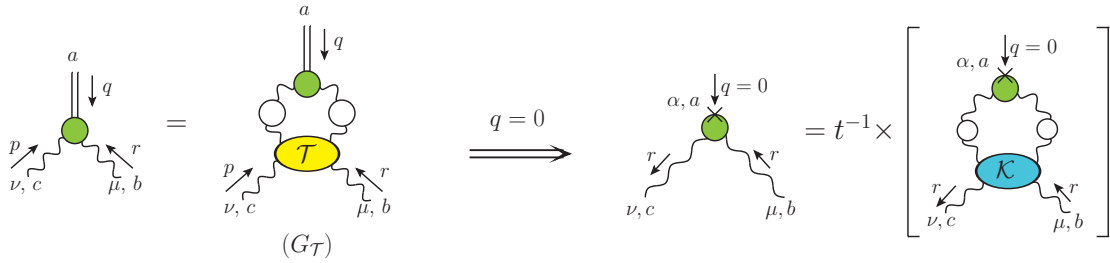


Figure 10. BSE for the effective vertex  $B_{\mu\nu}^{abc}(q, r, p)$  (left) and its  $q = 0$  limit (right).

## VI. DYNAMICAL SCALE-FIXING

In order to proceed further with our analysis, it is necessary to pass certain key equations to Euclidean space, following standard transformation rules. Specifically, we consider all physical momenta to be space-like; in particular,  $r^2 \rightarrow -r_E^2$ , where  $r_E^2 > 0$ . In addition, we use the conversion relations

$$\begin{aligned} \int_k &= i \int_{k_E}, & \Delta_E(r_E^2) &= -\Delta(-r_E^2), & \mathbb{B}_E(r_E^2) &= -\mathbb{B}(-r_E^2), \\ \mathbb{C}_E(r_E^2) &= -\mathbb{C}(-r_E^2), & L_{sg}^E(r_E^2) &= L_{sg}(-r_E^2). \end{aligned} \quad (6.1)$$

Applying the above relations to Eqs. (4.17), (5.8), and (5.9), the expressions for  $\omega_E$  and  $I_E$  read

$$\omega_E = \frac{3C_A}{2} \int_{k_E} k_E^2 \Delta_E^2(k_E) \mathbb{B}_E^2(k_E^2), \quad (6.2)$$

$$I_E = \frac{3C_A Z_3}{2} \int_{k_E} k_E^2 \Delta_E^2(k_E) \mathbb{B}_E(k_E^2). \quad (6.3)$$

The Euclidean versions of Eqs. (4.18) and (5.15) may be derived in a similar way. In doing so, note that the kernel  $K$  must be cast in the form<sup>4</sup>

$$K(r, k) = iK_{\mathbb{E}}(r_{\mathbb{E}}, k_{\mathbb{E}}), \quad (6.4)$$

where

$$i\alpha_s K_{\mathbb{E}}(r_{\mathbb{E}}, k_{\mathbb{E}}) := \frac{(r_{\mathbb{E}} \cdot k_{\mathbb{E}})}{c r_{\mathbb{E}}^2 k_{\mathbb{E}}^2} f^{abc} f^{amn} [P^{\mu\nu}(r) P^{\rho\sigma}(k) \mathcal{K}_{\rho\sigma\mu\nu}^{mncb}(-k, k, r, -r)]_{\mathbb{E}}, \quad (6.5)$$

and  $[\dots]_{\mathbb{E}}$  denotes the application of Eq. (6.1) to the expressions in square brackets.

Then, with  $t_{\mathbb{E}} := 1 - \omega_{\mathbb{E}}$ ,

$$\mathbb{B}_{\mathbb{E}}(r_{\mathbb{E}}^2) = t_{\mathbb{E}}^{-1} \alpha_s \int_{k_{\mathbb{E}}} k_{\mathbb{E}}^2 \Delta_{\mathbb{E}}^2(k_{\mathbb{E}}^2) K_{\mathbb{E}}(r_{\mathbb{E}}, k_{\mathbb{E}}) \mathbb{B}_{\mathbb{E}}(k_{\mathbb{E}}^2), \quad (6.6)$$

whereas the equation for  $L_{sg}^{\mathbb{E}}(r)$  reads

$$L_{sg}^{\mathbb{E}}(r_{\mathbb{E}}^2) = Z_3 + \alpha_s \int_{k_{\mathbb{E}}} k_{\mathbb{E}}^2 \Delta_{\mathbb{E}}^2(k_{\mathbb{E}}^2) K_{\mathbb{E}}(r_{\mathbb{E}}, k_{\mathbb{E}}) L_{sg}^{\mathbb{E}}(k_{\mathbb{E}}^2). \quad (6.7)$$

Finally, the expressions for the Euclidean displacement function and mass, retain the same form as in Eqs. (2.15) and (3.28), but now carry indices “E”, *i.e.*,

$$\mathbb{C}_{\mathbb{E}}(r_{\mathbb{E}}^2) := -I_{\mathbb{E}} \mathbb{B}_{\mathbb{E}}(r_{\mathbb{E}}^2), \quad m^2 = g^2 I_{\mathbb{E}}^2. \quad (6.8)$$

In order to simplify the notation, in what follows the index “E” will be omitted.

We next focus on the BSE of Eq. (6.6). Strictly speaking, Eq. (6.6) is a non-linear integral equation, due to the quadratic dependence of  $t$  on the unknown function  $\mathbb{B}$ . However, the fact that  $t$  is a constant, independent of the variable  $r$ , allows one to solve Eq. (6.6) as an eigenvalue problem, typical of a linear homogeneous equation, with one crucial difference: the solutions do not suffer from the scale indeterminacy intrinsic to such a linear equation, because the presence of  $t$  fixes the scale, up to an overall sign.

To appreciate the role played by the parameter  $t$ , we temporarily set  $t = 1$ . Then, let us suppose that the kernel  $K$  is such that the eigenvalue that yields a nontrivial solution for  $\mathbb{B}(k)$  requires that  $\alpha_s \rightarrow \alpha_*$ , where  $\alpha_*$  differs from the value predicted for  $\alpha_s$  within the renormalization scheme employed.

---

<sup>4</sup> The origin of the factor “ $i$ ” may be easily understood at the level of the one-gluon exchange diagram of Fig. 9; it is included in the definition of the gluon propagator, see Eq. (2.1).

Then, restoring  $t$  at the level of Eq. (5.15), it becomes clear that it has to compensate precisely for the difference between  $\alpha_s$  and  $\alpha_*$ . In particular, we must have

$$t = \frac{\alpha_s}{\alpha_*}, \quad (6.9)$$

which brings Eq. (5.15) into the required form

$$\mathbb{B}(r) = \alpha_* \int_k k^2 \Delta^2(k) K(r, k) \mathbb{B}(k). \quad (6.10)$$

To understand how the presence of the parameter  $t$  in Eq. (5.15) leads to the determination of the scale of  $\mathbb{B}(k)$ , note that, by combining Eqs. (5.10) and (6.9) we obtain the condition

$$\omega = 1 - \alpha_s/\alpha_*. \quad (6.11)$$

Since the value of the l.h.s. of Eq. (6.11) is fixed,  $\omega$  is completely determined, and, therefore, the size of the  $\mathbb{B}(k)$  entering in the definition of Eq. (6.2) is constrained.

To see this, let  $\mathbb{B}_0(k)$  be a solution of Eq. (5.15) with a scale set arbitrarily, *e.g.*, by imposing that the global maximum of  $\mathbb{B}_0(k)$  is at 1, and denote by  $\omega_0$  the value of  $\omega$  when  $\mathbb{B}(k) \rightarrow \mathbb{B}_0(k)$  is substituted in Eq. (6.2). The  $\mathbb{B}$  that is compatible with Eq. (6.11) is related to  $\mathbb{B}_0$  by a multiplicative constant,  $\sigma$ , *i.e.*,  $\mathbb{B}(k) = \sigma \mathbb{B}_0(k)$ , whose value is determined from the equation

$$\sigma^2 \omega_0 = 1 - \alpha_s/\alpha_*, \quad (6.12)$$

or, equivalently,

$$\sigma = \pm \sqrt{\frac{1 - \alpha_s/\alpha_*}{\omega_0}}. \quad (6.13)$$

Note that, since  $\omega$  is quadratic in  $\mathbb{B}(k)$ , the sign of  $\sigma$ , and hence the sign of  $\mathbb{B}$  itself, is left undetermined. However, as we can see from Eqs. (6.3) and (6.8),  $\mathbb{C}(k)$  is quadratic in  $\mathbb{B}(k)$ , and therefore does not get affected by the sign ambiguity of Eq. (6.13). In fact, the overall sign of  $\mathbb{C}(k)$  turns out to be negative for the entire range of Euclidean momenta, in agreement with the sign found in the lattice extraction of  $\mathbb{C}(k)$  presented in [59, 76].

## VII. RENORMALIZATION OF THE GLUON MASS EQUATION

The compact relation in Eq. (2.15) expresses the gluon mass in terms of the gluon-scalar transition amplitude  $I$ , which depends, in turn, on the BS amplitude  $\mathbb{B}(r)$ . After the

renormalization and the rotation to the Euclidean space,  $I$  is given by Eq. (6.3). The obvious difficulty associated with the use of the latter equation is the renormalization constant  $Z_3$  multiplying the relevant integral.

It turns out that a subtle sequence of relations allows one to implement the multiplicative renormalization implicit in Eq. (6.3) without having to carry out any integrations. The upshot of these considerations is that the renormalization of  $I$  finally amounts to the *effective* replacement  $Z_3 \rightarrow \omega L_{sg}(k)$  at the level of Eq. (6.3), *i.e.*,

$$I = \frac{3C_A}{2} \omega \int_k k^2 \Delta^2(k) L_{sg}(k) \mathbb{B}(k). \quad (7.1)$$

In what follows we will present a detailed derivation of the above key result.

The first observation is that, by virtue of Eq. (4.18), the  $Z_3$  in Eq. (4.17) may be substituted by the combination

$$Z_3 = L_{sg}(k) - \alpha_s \int_\ell \ell^2 \Delta^2(\ell) K(k, \ell) L_{sg}(\ell). \quad (7.2)$$

This procedure is typical when dealing with multiplicative renormalizability at the level of the SDEs, see, *e.g.*, [126], and is intimately connected with the so-called “skeleton expansion” of the SDE kernel.

The second observation is novel, and completely specific to the particular form of the BSE in Eq. (6.6). In particular, when the substitution of Eq. (7.2) is implemented, the BSE of Eq. (6.6) is triggered inside Eq. (6.3), leading to a crucial cancellation, and, finally, to Eq. (7.1).

In order to convey the underlying idea with a simple example, consider two functions  $g(x)$  and  $f(x)$ , satisfying the system of integral equations

$$g(x) = z + \int dy \tilde{g}(y) K(x, y), \quad f(x) = b^{-1} \int dy \tilde{f}(y) K(x, y), \quad (7.3)$$

where  $\tilde{g}(y) := g(y) u(y)$  and  $\tilde{f}(y) := f(y) u(y)$ , with  $u(y)$  a well-behaved function. The parameters  $z$  and  $b$  are real numbers, with  $b \neq 0, 1$ , and the limits of integration are arbitrary. Finally, the *common* kernel  $K(x, y)$  satisfies the symmetry relation  $K(x, y) = K(y, x)$ .

Let us further assume that the value of a constant  $\beta$  is given by the integral

$$\beta = z \int dx \tilde{f}(x). \quad (7.4)$$



The dependence of  $\beta$  on the parameter  $z$  may be eliminated in favor of the function  $g(x)$  by appealing to the system of Eq. (7.3). In particular, one employs the following sequence of steps

$$\begin{aligned}
\beta &= \int dx z \tilde{f}(x) \\
&= \int dx \left[ g(x) - \int dy \tilde{g}(y) K(x, y) \right] \tilde{f}(x) \\
&= \int dx g(x) \tilde{f}(x) - \int dx \int dy \tilde{g}(y) K(x, y) \tilde{f}(x) \\
&= \int dx \tilde{g}(x) \left[ f(x) - \underbrace{\int dy \tilde{f}(y) K(x, y)}_{bf(x)} \right], \tag{7.5}
\end{aligned}$$

where in the second line we used the first relation in Eq. (7.3), while in the last line the relabelling  $x \leftrightarrow y$  of the integration variables was carried out, the symmetry of the kernel  $K(x, y)$  was exploited, and the second relation in Eq. (7.3) was invoked. Thus, one obtains

$$\beta = (1 - b) \int dx \tilde{f}(x) g(x), \tag{7.6}$$

where we used that  $\tilde{g}(x)f(x) = \tilde{f}(x)g(x)$ . Evidently, the dependence of  $\beta$  on the parameter  $z$  has been exchanged for the dependence on the function  $g(x)$ , which was absent from the original integral in Eq. (7.4). In Appendix A, we present a concrete example, where the equivalence between Eqs. (7.4) and (7.6) may be worked out exactly.

At this point it is straightforward to repeat the construction leading to Eq. (7.6) for the system of integral equations given by Eqs. (6.6) and (6.7), in conjunction with Eq. (6.3). To that end, all we need is to establish the correspondence

$$\begin{aligned}
\{g(x), f(x), u(x), K(x, y)\} &\leftrightarrow \{L_{sg}(r), \mathbb{B}(r), k^2 \Delta^2(k), \alpha_s K(r, k)\}, \\
\{\beta, z, b, dx, dy\} &\leftrightarrow \{2I/3C_A, Z_3, t, d^4k, d^4\ell\}. \tag{7.7}
\end{aligned}$$

In particular, with the above identifications and Eq. (5.10), we find that the analogue of Eq. (7.6) is precisely Eq. (7.1), which is the announced result. The diagrammatic representation of the steps described in Eq. (7.5) is shown in Fig. 11; note that, in doing so, we employ the representation of the BSE given in Fig. 10, whose main building block was introduced in Fig. 6.

The above construction reveals a striking fact: if the parameter  $\omega$  is set to zero, the cancellation described in Eq. (7.5) [Fig. 11] is perfect; thus, even if a non-trivial  $\mathbb{B}$  is obtained

$$\begin{aligned}
4\delta^{ab}I_R &= \text{Diagram 1} \\
&= \left[ \text{Diagram 2} - \text{Diagram 3} \right] \text{Diagram 4} \\
&= \text{Diagram 5} \left[ \text{Diagram 6} - \text{Diagram 7} \right] \\
&= \omega \times \left[ \text{Diagram 8} \right]
\end{aligned}$$

Figure 11. Diagrammatic illustration of the renormalization of  $I$ . Note that the diagrams containing the kernel  $\mathcal{K}$  undergo a relabeling of integration momenta,  $k \leftrightarrow \ell$ , from the second to the third line.

from Eq. (6.6), the renormalized transition amplitude  $I$ , and therefore, the gluon mass  $m$ , vanish. In that sense, the gluon mass emerges due to the mismatch between the kernels in the equations for  $\mathbb{B}$  and  $L_{sg}(r)$ , [see Eqs. (6.6) and (6.7)], produced by the presence of a  $t \neq 1$  in the former but not in the latter. In diagrammatic terms, the non-vanishing of the gluon mass hinges on the difference between the  $\mathcal{T}$  appearing in Fig. 10 and the  $\mathcal{K}$  in Fig. 8, namely the component  $\mathcal{M}$  [see Fig. 3]. Even though, on intuitive grounds, the importance of this term seems evident, given that it carries precisely the information about the emergence of a massless scalar, the quantitative understanding attained through the above construction is most valuable.

Quite interestingly, the cancellations described in Eq. (7.5) are not coincidental, but are rather driven by an underlying mathematical principle. In particular, as we discuss in detail in the next section, our SDE-BSE analysis may be interpreted as a rather subtle application of the so-called “Fredholm alternatives theorem”.

### VIII. FREDHOLM ALTERNATIVES THEOREM AND ITS EVASION

Let us consider the inhomogeneous and homogeneous Fredholm equations of the second kind, given by [96, 97]

$$f_1(x) = f_2(x) + \lambda \int_a^b K(x, y) f_1(y) dy, \quad (8.1)$$

and

$$f_3(x) = \lambda \int_a^b K(x, y) f_3(y) dy, \quad (8.2)$$

respectively. Here,  $f_1$  and  $f_3$  are the unknown functions, while  $f_2$  is a known inhomogeneous term. The kernel,  $K(x, y)$ , is assumed to be continuous and square-integrable in the interval  $[a, b]$ , in which case it is said to be a Hilbert-Schmidt integral operator.

The Fredholm alternatives theorem imposes restrictions on the existence of simultaneous solutions of Eqs. (8.1) and (8.2). For the purposes of the present work, it suffices to consider the special case of the theorem when  $K(x, y)$  is real and symmetric in  $x \leftrightarrow y$ <sup>5</sup>. Under these simplifications, the Fredholm alternatives theorem can be stated as follows [97]:

- (a) If  $\lambda$  is not an eigenvalue of  $K(x, y)$ , *i.e.*, if the homogeneous equation has only the trivial solution,  $f_3(x) = 0$ , then the inhomogeneous Eq. (8.1) has a solution for *any* nonzero  $f_2(x)$ .
- (b) If  $\lambda$  is an eigenvalue of  $K(x, y)$ , such that  $f_3(x)$  is nonvanishing, then Eq. (8.1) has solutions *if and only if*

$$\int_a^b f_2(y) f_3(y) dy = 0. \quad (8.3)$$

In order to connect the Fredholm alternative theorem to the system of equations satisfied by  $L_{sg}(r)$  and  $\mathbb{B}(r)$ , we need to perform certain transformations that will bring Eqs. (6.6) and (6.7) to a form similar to Eqs. (8.1) and (8.2).

We begin by rewriting Eqs. (6.6) and (6.7) in spherical coordinates. To this end, we define the variables

$$x := r^2, \quad y := k^2, \quad (8.4)$$

and the angle  $\theta$  between  $r$  and  $k$ , *i.e.*,  $r \cdot k = |r||k|c_\theta$ , where we use the shorthand notation  $c_\theta := \cos \theta$  and  $s_\theta := \sin \theta$ . Note that the kernel  $K(r, k)$  is a function of  $x$ ,  $y$ , and  $\theta$ , *i.e.*,  $K(r, k) \equiv K(x, y, \theta)$ .

<sup>5</sup> For the generalization of the theorem for a complex and non-symmetric kernel see, *e.g.*, [96, 97].

Moreover, we introduce an ultraviolet momentum cutoff,  $\Lambda$ , to regularize potential divergences<sup>6</sup>. In this case, the integral measure takes the form

$$\int_k := \frac{1}{(2\pi)^3} \int_0^{\Lambda^2} dy y \int_0^\pi d\theta s_\theta^2. \quad (8.5)$$

Now, the only dependence of the integrands of Eqs. (6.6) and (6.7) on the angle is through  $K(x, y, \theta)$ . Then, we can define an ‘‘angle-integrated kernel’’,  $\widehat{K}(x, y)$ , by

$$\widehat{K}(x, y) = \frac{1}{(2\pi)^3} \int_0^\pi d\theta s_\theta^2 K(x, y, \theta). \quad (8.6)$$

With the above definitions, Eqs. (6.6) and (6.7) are recast as

$$\begin{aligned} \mathbb{B}(x) &= t^{-1} \alpha_s \int_0^{\Lambda^2} dy \mathcal{Z}^2(y) \widehat{K}(x, y) \mathbb{B}(y), \\ L_{sg}(x) &= Z_3 + \alpha_s \int_0^{\Lambda^2} dy \mathcal{Z}^2(y) \widehat{K}(x, y) L_{sg}(y), \end{aligned} \quad (8.7)$$

where we introduced the gluon dressing function,  $\mathcal{Z}(x) := x\Delta(x)$ .

At this point, we note that since  $K(r, k)$  is symmetric under the exchange of  $r \leftrightarrow k$ , then  $\widehat{K}(x, y) = \widehat{K}(y, x)$ . However, the complete kernel of Eq. (8.7), namely  $\mathcal{Z}^2(y)\widehat{K}(x, y)$ , is not symmetric under  $x \leftrightarrow y$ , due to the factor of  $\mathcal{Z}^2(y)$ . Nevertheless, it can be transformed into an equivalent system of equations with a symmetric kernel.

To this end, we multiply Eq. (8.7) by  $\mathcal{Z}(x)$ , and define

$$\widetilde{\mathbb{B}}(x) := \mathcal{Z}(x)\mathbb{B}(x), \quad \widetilde{L}_{sg}(x) := \mathcal{Z}(x)L_{sg}(x), \quad \widetilde{K}(x, y) := \mathcal{Z}(x)\mathcal{Z}(y)\widehat{K}(x, y). \quad (8.8)$$

Then, Eq. (8.7) is equivalent to

$$\begin{aligned} \widetilde{\mathbb{B}}(x) &= t^{-1} \alpha_s \int_0^{\Lambda^2} dy \widetilde{K}(x, y) \widetilde{\mathbb{B}}(y), \\ \widetilde{L}_{sg}(x) &= Z_3 \mathcal{Z}(x) + \alpha_s \int_0^{\Lambda^2} dy \widetilde{K}(x, y) \widetilde{L}_{sg}(y), \end{aligned} \quad (8.9)$$

whose kernel  $\widetilde{K}(x, y)$  is symmetric.

Finally, the Eq. (6.3) for  $I$  can be recast as

$$I = \frac{3C_A Z_3}{32\pi^2} \int_0^{\Lambda^2} dy \mathcal{Z}(y) \widetilde{\mathbb{B}}(y). \quad (8.10)$$

---

<sup>6</sup> For the sake of simplicity, a hard cutoff has been employed; we have confirmed that exactly the same conclusions are reached when the calculation is carried out using dimensional regularization.

The implications of the Fredholm alternatives theorem for Eq. (8.9) are now straightforward to establish. Specifically, suppose that  $\omega = 0$ , such that  $t = 1$ . Then, we have a direct correspondence between Eq. (8.9) and the Eqs. (8.1) and (8.2) through the identification

$$\begin{aligned} \{f_1(x), f_2(x), f_3(x), K(x, y)\} &\leftrightarrow \{\tilde{L}_{sg}(x), Z_3 \mathcal{Z}(x), \tilde{\mathbb{B}}(x), \tilde{K}(x, y)\}, \\ \{\lambda, a, b\} &\leftrightarrow \{\alpha_s, 0, \Lambda^2\}. \end{aligned} \quad (8.11)$$

Hence, for both  $L_{sg}(x)$  and  $\mathbb{B}(x)$  to be nonzero, the Fredholm alternatives theorem implies that

$$Z_3 \int_0^{\Lambda^2} dy \mathcal{Z}(y) \tilde{\mathbb{B}}(y) = 0. \quad (8.12)$$

Comparison to Eq. (8.10) then yields  $I = 0$ , and therefore, due to Eq. (2.15),  $m^2 = 0$ .

We conclude that the generation of a gluon mass through the SM hinges on  $\omega \neq 0$ ,  $t \neq 1$ , which leads to the evasion of Fredholm alternatives theorem, by relaxing the assumption of equal kernels in Eq. (8.9). Otherwise, if  $\omega = 0$ , the theorem imposes a vanishing gluon mass, even in the presence of a nonvanishing  $\mathbb{B}$ , because, quite remarkably, the condition of Eq. (8.3) is *precisely* the equation for the transition amplitude  $I$ .

Let us finally discuss a subtlety related to the applicability of Fredholm's theorem in the present context. Specifically, the theorem applies to a system of *linear* equations, whereas the kernel  $K(r, k)$  depends on  $L_{sg}(r)$  [see Fig. 9 and Eq. (9.6)]. In that sense, even for  $\omega = 0$ , the equation for  $L_{sg}(r)$  is nonlinear. Nevertheless, our main conclusion, namely that for  $\omega = 0$  the gluon mass vanishes, persists.

To see this, suppose there exists a solution,  $L_0(r)$  and  $\mathbb{B}_0(r)$ , to the full nonlinear system of equations. Then, let  $K_0(r, k)$  be the value of  $K(r, k)$  obtained by the substitution of  $L_{sg} \rightarrow L_0$  in its expression<sup>7</sup>. Now,  $L_0(r)$  and  $\mathbb{B}_0(r)$  must also be a solution of

$$\begin{aligned} L_{sg}(r) &= Z_3 + \alpha_s \int_k k^2 \Delta^2(k^2) K_0(r, k) L_{sg}(k), \\ \mathbb{B}(r) &= t^{-1} \alpha_s \int_k k^2 \Delta^2(k^2) K_0(r, k) \mathbb{B}(k), \end{aligned} \quad (8.13)$$

since setting  $\{L_{sg}, \mathbb{B}\} \rightarrow \{L_0, \mathbb{B}_0\}$  in the above equation recovers the original, nonlinear, system. But the Fredholm alternatives theorem applies to Eq. (8.13) with  $\omega = 0$ , in which case the arguments of Sec. VIII lead to  $m = 0$ . Hence, the nonlinear nature of the equations

---

<sup>7</sup> As can be seen from Fig. 9, the  $L_{sg}$  enters in  $K(r, k)$  in such a way that the symmetry under  $r \leftrightarrow k$  is preserved.

cannot by itself evade the Fredholm alternatives theorem when  $\omega = 0$  and the conclusion of our analysis is unaffected.

## IX. NUMERICAL ANALYSIS

In this section we explore the numerical implications of the main results presented so far, placing particular emphasis on the value of the gluon mass  $m$ , and the shape and size of the displacement function  $\mathbb{C}(r)$ . In doing so, we will use two important results as benchmarks for these quantities. In particular, we identify as the optimal value for the gluon mass the inverse of the saturation point of the lattice gluon propagator at the origin. Evidently, this is a renormalization-point dependent mass scale, and does not admit a direct physical interpretation<sup>8</sup>; when the lattice curve has been renormalized such that  $\Delta^{-1}(\mu^2) = \mu^2$  at  $\mu = 4.3$  GeV, one obtains the value  $m_{\text{lat}} = 354$  MeV [106]. As for the displacement function, we will compare our results with the curve shown in the left panel of Fig. 15, which was obtained following the method outlined in Sec. III D; for details, see [76].

The main steps of the numerical procedure followed may be summarized as follows:

(i) Since the four-gluon kernel  $K(r, k)$  entering in BSE of Eq. (6.6) is not known, we resort to models for it, using its one-gluon exchange approximation,  $K_{\text{oge}}(r, k)$ , as our point of departure. Specifically, at the beginning of the numerical procedure, an *Ansatz* for  $K(r, k)$  is constructed, by varying the parameters of  $K_{\text{oge}}(r, k)$ .

(ii) The  $K(r, k)$  from the previous step is fed into the BSE of Eq. (6.6), which is solved as an eigenvalue problem, yielding a solution for  $\mathbb{B}(r)$ . The corresponding eigenvalue  $\alpha_*$  is used in Eq. (6.13) to determine the value of  $\sigma$ , thus fixing the scale of  $\mathbb{B}(r)$ . In addition, the value of  $\omega$  is obtained directly from Eq. (6.11).

(iii) The above solution for  $\mathbb{B}(r)$  is substituted into Eq. (7.1) to yield the value of  $I$ . Then, using the two relations in Eq. (6.8), we get the value of the gluon mass and the form of the displacement function, and compare them with the benchmark results.

(vi) The procedure is repeated, using a different model for the kernel  $K(r, k)$ .

---

<sup>8</sup> An RGI gluon mass of about 450 MeV may be obtained following the procedure described in [72, 127].

### A. One-gluon exchange approximation of the BSE kernel

For practical calculations, the kernel  $\mathcal{K}_{\rho\sigma\mu\nu}^{mabc}(-k, k, r, -r)$  of the BSE must be truncated. To this end, we start with the skeleton expansion of  $\mathcal{K}_{\rho\sigma\mu\nu}^{mabc}(-k, k, r, -r)$ , shown in Fig. 9, which we write as

$$\mathcal{K}_{\rho\sigma\mu\nu}^{mabc}(-k, k, r, -r) = \sum_{i=1}^{\infty} (b_i)_{\rho\sigma\mu\nu}^{mabc}(-k, k, r, -r). \quad (9.1)$$

Substituting Eq. (9.1) into Eq. (6.5), we can compute the contribution of each diagram ( $b_i$ ) to the Euclidean  $K(r, k)$  entering Eq. (6.6). As it turns out, the diagram ( $b_2$ ), which is simply the tree-level four-gluon vertex, vanishes when inserted in Eq. (6.5) [55, 58], *i.e.*,

$$f^{abc} f^{amn} P^{\mu\nu}(r) P^{\rho\sigma}(k) (b_2)_{\rho\sigma\mu\nu}^{mabc}(-k, k, r, -r) = 0. \quad (9.2)$$

Hence,  $K(r, k)$  reads

$$K(r, k) = K_{\text{oge}}(r, k) + K_{\text{ho}}(r, k), \quad (9.3)$$

where  $K_{\text{oge}}(r, k)$  is the contribution of the one-gluon exchange diagram, ( $b_1$ ), and  $K_{\text{ho}}(r, k)$  represent the higher-order diagrams ( $b_i$ ) with  $i \geq 3$ .

Next, we focus on the one-gluon exchange contribution,  $K_{\text{oge}}(r, k)$ . From diagram ( $b_1$ ) of Fig. 9 and Eq. (6.5), one obtains in the Landau gauge

$$K_{\text{oge}}(r, k) = \frac{2\pi C_A}{3} \Delta(k-r) \left[ \bar{\Gamma}_{\mu\rho\sigma}(r, -k, k-r) \bar{\Gamma}^{\mu\rho\sigma}(-r, k, r-k) \right]_{\text{E}}, \quad (9.4)$$

where

$$\bar{\Gamma}_{\mu\rho\sigma}(r, -k, k-r) := P_{\mu}^{\mu'}(r) P_{\rho}^{\rho'}(k) P_{\sigma}^{\sigma'}(k-r) \Pi_{\mu'\rho'\sigma'}(r, -k, k-r), \quad (9.5)$$

is the transversely projected three-gluon vertex [53, 73, 74, 105, 110, 116, 128–130].

In principle, the  $\bar{\Gamma}_{\mu\rho\sigma}$  appearing in Eq. (9.4) consists of four independent tensor structures, each accompanied by a form factor that depends on three kinematic variables. However, as has been shown in numerous recent works [53, 73, 74, 105, 110, 116, 128–131], the classical tensor structure of  $\bar{\Gamma}_{\mu\rho\sigma}$  is dominant, and the associated form factor  $L_{sg}$  may be accurately described as a function of a single special kinematic variable, denoted by  $s^2$ , namely

$$\bar{\Gamma}^{\mu\rho\sigma}(r, -k, k-r) = \bar{\Gamma}_0^{\mu\rho\sigma}(r, -k, k-r) L_{sg}(s), \quad s^2 := \frac{1}{2}[r^2 + k^2 + (k-r)^2], \quad (9.6)$$

where  $\bar{\Gamma}_0^{\mu\rho\sigma}$  is the tree-level value of  $\bar{\Gamma}^{\mu\rho\sigma}$ , obtained by substituting the  $\Pi^{\mu'\rho'\sigma'}$  in Eq. (9.5) by the  $\Pi_0^{\mu'\rho'\sigma'}$  of Eq. (2.5).

Then, using Eq. (9.6), employing spherical coordinates, and introducing the variables defined in Eq. (8.4), one obtains

$$K_{\text{oge}}(x, y, \theta) = K_{\text{kin}}(x, y, \theta) \mathcal{R}_{\text{oge}}(u, s), \quad (9.7)$$

where  $u^2 := (k - r)^2 = x + y - 2c_\theta \sqrt{xy}$ ,  $s^2 = x + y - c_\theta \sqrt{xy}$ ,

$$K_{\text{kin}}(x, y, \theta) := \frac{8\pi C_A}{3u^2 \sqrt{xy}} \left\{ c_\theta s_\theta^2 \left[ (c_\theta^2 + 8)xy - 6c_\theta \sqrt{xy}(x + y) + 3(x^2 + y^2) \right] \right\}, \quad (9.8)$$

and

$$\mathcal{R}_{\text{oge}}(u, s) := \Delta(u) L_{sg}(s). \quad (9.9)$$

The ingredients entering in the  $K_{\text{oge}}(x, y, \theta)$  of Eq. (9.7) are all accurately known from lattice simulations. In particular, we use for  $\Delta(u)$  and  $L_{sg}(s)$  the fits to the lattice results of [106], given by Eqs. (C.11) and (C.12) of [59], respectively; the corresponding curves are shown in Fig. 12. Note that these ingredients are renormalized in the so-called ‘‘asymmetric MOM scheme’’ [102, 103, 105, 106, 116], defined by the renormalization condition

$$\Delta^{-1}(\mu) = \mu^2, \quad L_{sg}(\mu) = 1, \quad (9.10)$$

with  $\mu = 4.3$  GeV denoting the renormalization point. For this renormalization scheme and point, the corresponding strong charge takes the value  $\alpha_s = 0.27$  [103], which we adopt from now on.

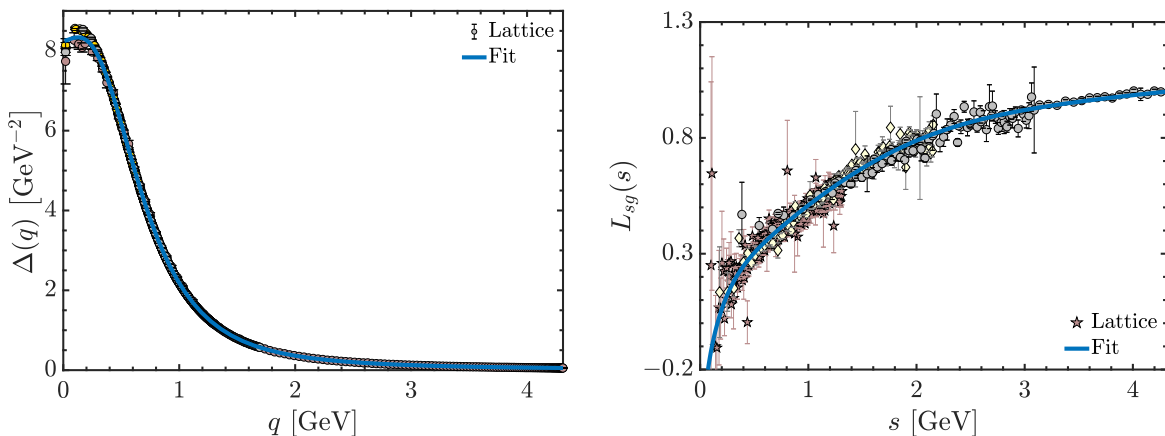


Figure 12. Lattice data (points) for the gluon propagator from [106] (left) and the three-gluon vertex form factor,  $L_{sg}(s)$ , from [105] (right). The blue continuous curves represent the corresponding fits given by Eqs. (C11) and (C12) of [59].



## B. Asymptotic behavior of $\mathbb{B}(r)$

For a given kernel,  $K(r, k)$ , the eigenvalue problem of Eq. (6.10) can be solved with standard procedures, such as *Nyström's* method [132]. This determines the eigenvalue,  $\alpha_*$ , and an eigenfunction,  $\mathbb{B}_0(r)$ , arbitrarily normalized such that its global maximum is 1. In order to fix the physical scale of  $\mathbb{B}(r)$  and compute the gluon mass, we then need to compute  $\omega$  and  $I$  through Eqs. (6.2) and (7.1). This task requires an analysis of the ultraviolet behavior of the integrals in the latter equations, which we describe in detail below. For simplicity, we will illustrate the procedure with the case of the one-gluon exchange kernel,  $K_{\text{oge}}$ , but it applies equally to the kernels constructed through Eq. (9.17).

Let us begin by writing Eqs. (6.2) and (7.1) in spherical coordinates,

$$\omega = \lambda \int_0^\infty dy y^2 \Delta^2(y) \mathbb{B}^2(y), \quad (9.11)$$

$$I = \lambda \omega \int_0^\infty dy y^2 \Delta^2(y) L_{sg}(y) \mathbb{B}(y), \quad (9.12)$$

where  $\lambda := 3C_A/(32\pi^2)$ .

In addition, let us recall that at large momenta  $\Delta(y)$  and  $L_{sg}(y)$  approach their one-loop resummed perturbative behaviors [60, 73, 133–136]

$$\Delta(y) \sim y^{-1} L_{\text{UV}}^{-13/22}(y), \quad L_{sg}(y) \sim L_{\text{UV}}^{17/44}(y), \quad L_{\text{UV}}(y) := c \ln(y/\Lambda_{\text{MOM}}^2), \quad (9.13)$$

where  $c = 1/\ln(\mu^2/\Lambda_{\text{MOM}}^2)$ , and  $\Lambda_{\text{MOM}}$  is the (quenched) QCD mass-scale in the MOM scheme [137–140]; we employ the one-loop result  $\Lambda_{\text{MOM}}^2 = \mu^2 \exp[-12\pi/(11C_A\alpha_s)]$ , for which  $\Lambda = 520$  MeV and  $c = 0.236$ . Note that the fits of Eqs. (C.11) and (C.12) of [59] for  $\Delta(r)$  and  $L_{sg}(r)$  reproduce Eq. (9.13) by construction.

Now, the asymptotic behavior of  $\mathbb{B}_0(r)$  is not known analytically. Nevertheless, the numerical solutions for  $\mathbb{B}_0(r)$  are found to be accurately approximated by the asymptotic form

$$\lim_{r \rightarrow \infty} \mathbb{B}_0(r) = \frac{a}{r^2 L_{\text{UV}}^\kappa(r^2)}, \quad (9.14)$$

for  $r > 5$  GeV, where the constants  $a$  and  $\kappa$  can be determined by fitting the  $\mathbb{B}_0(r)$  data in this range. In Fig. 13 this is shown explicitly for the case when  $K(r, k) = K_{\text{oge}}(r, k)$ , with the blue continuous curve showing the full solution  $\mathbb{B}_0(r)$ , whereas the orange dot-dashed represents Eq. (9.14) with  $a = 3.17$  and  $\kappa = 0.958$ . The corresponding eigenvalue is  $\alpha_* = 0.685$ .

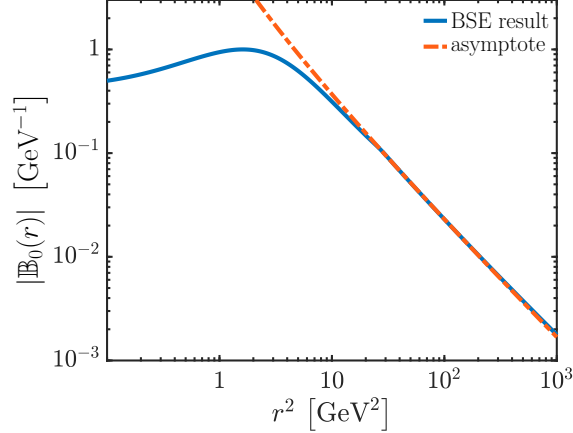


Figure 13. Absolute value of the eigenfunction  $\mathbb{B}_0(r)$  obtained with the one-gluon exchange kernel,  $K_{\text{oge}}(r, k)$ , normalized such that it has 1 as global maximum (blue continuous). The orange dot-dashed line corresponds to the asymptotic form of Eq. (9.14), and accurately approximates  $\mathbb{B}_0(r)$  for  $r^2 > 25 \text{ GeV}^2$ .

Next, to get  $\omega_0$ , we set  $\mathbb{B} \rightarrow \mathbb{B}_0$  into Eq. (9.11). With the aid of Eqs. (9.13) and (9.14), it is easy to establish that the integral converges rapidly, and its numerical evaluation is rather straightforward, yielding  $\omega_0 = 0.389$ .

In contrast, the expression for  $I$  given in Eq. (9.12) is found to converge slowly, requiring a more careful treatment.

To analyze the ultraviolet convergence of Eq. (9.12), we first separate the integration interval in two parts, by means of a large momentum scale,  $M^2$ , *i.e.*,

$$I = \underbrace{\lambda\omega \int_0^{M^2} dy y^2 \Delta^2(y) L_{sg}(y) \mathbb{B}(y)}_{I_{\text{IR}}} + \underbrace{\lambda\omega \int_{M^2}^{\infty} dy y^2 \Delta^2(y) L_{sg}(y) \mathbb{B}(y)}_{I_{\text{UV}}}. \quad (9.15)$$

For  $M$  sufficiently large, all of the inputs in  $I_{\text{UV}}$  can be substituted by their asymptotic forms, namely Eqs. (9.13) and (9.14). The resulting integral can then be done analytically,

$$I_{\text{UV}} \sim \sigma a \lambda \omega \int_{M^2}^{\infty} dy \frac{1}{y L_{\text{UV}}^{\kappa+35/44}(y)} = \frac{\sigma a \lambda \omega}{c^{\kappa+35/44} (\kappa - 9/44) \ln^{\kappa-9/44}(M^2/\Lambda_{\text{MOM}}^2)}, \quad (9.16)$$

provided that  $\kappa > 9/44 = 0.204$ , which we find to be satisfied by our numerical solutions for  $\mathbb{B}(r)$ .

However, the convergence of Eq. (9.16) is slow, and direct numerical integration of Eq. (9.12) becomes unreliable. Instead, in what follows we use Eq. (9.15) with  $M = 5 \text{ GeV}$ , and compute  $I$  in two steps: first,  $I_{\text{IR}}$  is calculated by direct numerical integration of the

interpolated data for  $\mathbb{B}(r)$ ; then,  $I_{UV}$  is approximated by Eq. (9.16), and evaluated with the previously determined values of  $a$ ,  $\kappa$  and  $\sigma$ . Finally, this procedure yields  $I = \pm 0.689$  GeV.

Then, using Eq. (6.8), we obtain  $m = 1.27$  GeV, and the resulting displacement function  $\mathbb{C}(r)$  is shown as a yellow dashed curve in Fig. 15. Evidently, both findings are considerably larger than the results obtained from the lattice analysis of [76, 106] for  $\{m_{\text{lat}}, \mathbb{C}_{\text{lat}}(r)\}$ . This, in turn, motivates the study of the potential impact that the form of the kernel may have on these quantities.

### C. Varying the BSE kernel

In this subsection, we modify the form of the BSE kernel for the purpose of reaching a better agreement with the lattice results.

It is clear that, in order to determine the effect of the higher-order diagrams comprising  $K_{\text{ho}}(r, k)$ , one has to carry out extensive calculations. Instead, in the present analysis we simply treat the full  $K(r, k)$  as a deformation of the one-gluon exchange  $K_{\text{oge}}(r, k)$ , obtained by varying the function  $\Delta(u)$  entering in Eq. (9.7). We emphasize that this is the only place where this function is varied; everywhere else,  $\Delta$  retains its standard form.

Specifically, in the kernel of the BSE for  $\mathbb{B}(r)$ , see Eq. (8.5), we set

$$K(x, y, \theta) \rightarrow K_{\text{eff}}(x, y, \theta) = K_{\text{kin}}(x, y, \theta) \mathcal{R}_{\text{eff}}(u, s), \quad (9.17)$$

where the function  $\mathcal{R}_{\text{eff}}(u, s)$  is given by

$$\mathcal{R}_{\text{eff}}(u, s) = \Delta_{\text{eff}}(u) L_{sg}(s), \quad (9.18)$$

with  $\Delta_{\text{eff}}(u)$  parametrized as

$$\Delta_{\text{eff}}(u) = \Delta(u) \times \left[ 1 + \frac{c_0 u^2}{1 + c_1 u^2 + c_2 u^4} \right]. \quad (9.19)$$

Note that  $K_{\text{oge}}$  is recovered by setting  $c_0 = 0$  in Eq. (9.19). Moreover, at large momenta,  $\Delta_{\text{eff}}(u)$  reduces to  $\Delta(u)$ , such that the  $K_{\text{eff}}$  reduce to  $K_{\text{oge}}$ .

We next vary the  $c_i$  in Eq. (9.19) within certain intervals, and consider the resulting behaviour of  $\{m, \mathbb{C}\}$ . Upon systematic inspection of the parameter space, we conclude that the best values for  $c_1$  and  $c_2$  are  $c_1 = 0.00667$  GeV<sup>-2</sup> and  $c_2 = 0.0486$  GeV<sup>-4</sup>; we therefore keep  $c_1$  and  $c_2$  fixed at these values, and only vary  $c_0$ .

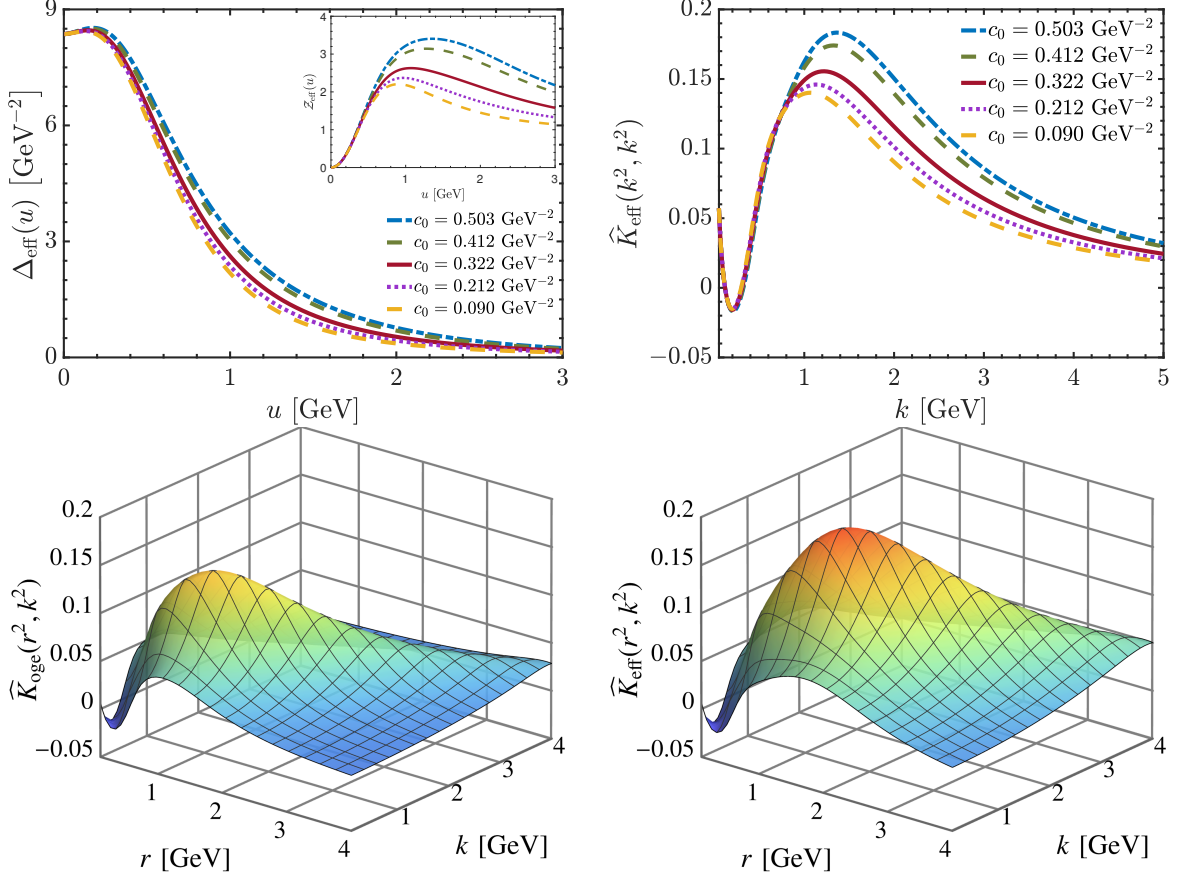


Figure 14. Top left: A family of variations of  $\Delta_{\text{eff}}(u)$ , obtained by varying the parameter  $c_0$  in Eq. (9.19). The inset shows the corresponding dressing functions,  $\mathcal{Z}_{\text{eff}}(q) := q^2 \Delta_{\text{eff}}(q)$ . Top right: Diagonal  $\widehat{K}_{\text{eff}}(k^2, k^2)$  of the angular-integrated kernel  $\widehat{K}_{\text{eff}}(r^2, k^2)$ , defined by Eq. (8.6), corresponding to the family of  $\Delta_{\text{eff}}(u)$  on the left panel. Bottom: General kinematics  $\widehat{K}(r^2, k^2)$  for  $K \rightarrow K_{\text{ogee}}$  (left),  $K \rightarrow K_{\text{eff}}$  (right). Note that the maximum of  $K_{\text{eff}}$  is enhanced by about 30% with respect to that of  $\widehat{K}_{\text{ogee}}$ .

On the top left panel of Fig. 14 we show the family of  $\Delta_{\text{eff}}(r)$  obtained by varying  $c_0$  within the interval  $[0, 0.503] \text{ GeV}^{-2}$ , while on the top right panel the diagonals ( $r^2 = k^2$ ) of the resulting  $\widehat{K}_{\text{eff}}(r^2, k^2)$  are displayed. As we see, enhancing  $\Delta_{\text{eff}}(u)$  leads to an enhancement of  $\widehat{K}_{\text{eff}}(r^2, k^2)$ . In the bottom panel one may see how the entire shape of the angular-integrated kernel gets modified when  $c_0$  varies from  $c_0 = 0$ , corresponding to the  $\widehat{K}_{\text{ogee}}(r^2, k^2)$ , to the case  $c_0 = 0.503 \text{ GeV}^{-2}$ . Note, in particular, that the maximum of  $\widehat{K}_{\text{eff}}(r^2, k^2)$  is enhanced by about 30% with respect to that of  $\widehat{K}_{\text{ogee}}$ .

Next, we compute the values of  $m$  and  $\mathbb{C}(r)$  corresponding to the family of  $\Delta_{\text{eff}}(u)$  of

Fig. 14. The resulting displacement amplitudes are shown on the left panel of Fig. 15, with the corresponding values of  $m$  given in the legend.

Note that, for  $c_0 = 0.212 \text{ GeV}^{-2}$  (red continuous curve on the panel of Fig. 15), the resulting  $\mathbb{C}(r)$  is statistically consistent with  $\mathbb{C}_{\text{lat}}(r)$ ; however, for this value of  $c_0$ , the mass turns out to be  $m = 687 \text{ MeV}$ , nearly twice the value of  $m_{\text{lat}}$ . Variation of the remaining parameters of Eq. (9.19) show the same pattern: improving the agreement between  $\mathbb{C}(r)$  and  $\mathbb{C}_{\text{lat}}(r)$  causes  $m$  to exceed  $m_{\text{lat}}$ .

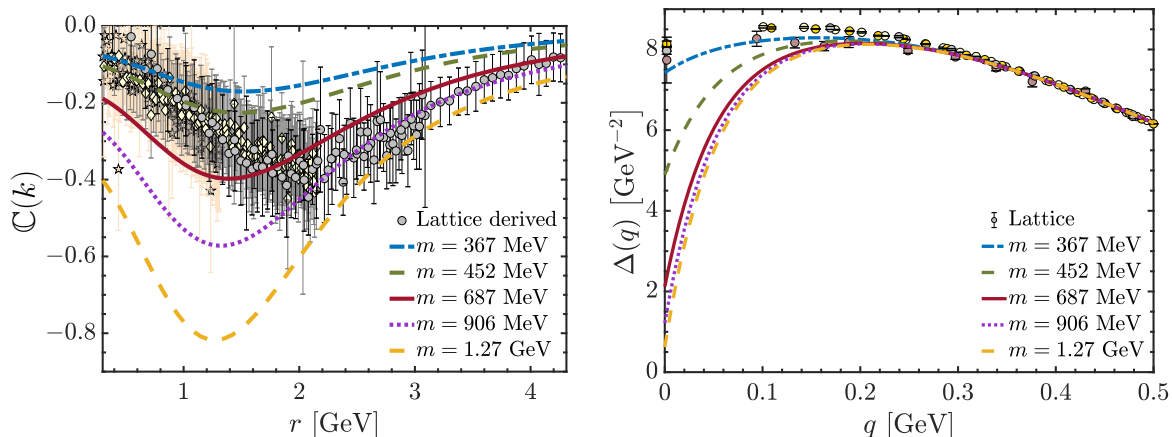


Figure 15. Left: Displacement amplitude,  $\mathbb{C}(r)$ , for different values of the parameter  $c_0$  (see legends of Fig. 14) of Eq. (9.19). The lattice-derived results of [76] are shown as points for comparison. Note that the red dashed line lies entirely within the errors of  $\mathbb{C}_{\text{lat}}(r)$ . Right: Gluon propagator,  $\Delta(q)$ , for different masses, assuming the functional form of Eq. (9.20), compared to the lattice data of [106].

Lastly, we illustrate the effect of the masses obtained in the Fig. 15 on the gluon propagator. Evidently, determining  $\Delta(q)$  self-consistently requires solving the coupled system of equations comprised by the gluon propagator and three-gluon vertex SDEs, which is beyond the scope of the present study. Instead, we assume that  $\Delta(q)$  is modified only near the origin by the value of  $m$ , recovering the lattice results for large  $q$ . A functional form that implements this assumption is

$$\Delta(q) = \Delta_{\text{fit}}(q) - [\Delta_{\text{fit}}(0) - 1/m^2] \exp(-q/\nu), \quad (9.20)$$

where  $\nu = 0.05 \text{ GeV}$ , and  $\Delta_{\text{fit}}(q)$  is the fit to the lattice data of [106] given by Eq. (C.11) of [59]. The resulting curves are shown on the right panel of Fig. 15.

## X. DISCUSSION AND CONCLUSIONS

In the present work we have addressed important open issues related to the implementation of the SM in a non-Abelian context. In particular, the question of how the scale of the gluon mass may be fixed has been solved, at least in principle, by introducing a nonlinear component into the BSE that controls the bound state amplitude,  $\mathbb{B}(r)$ , of the massless pole formation. In addition, we have put forth a novel approach for dealing with the problem of the multiplicative renormalizability of the gluon mass equation, thus reaching a manifestly finite answer for the gluon mass. The success of this renormalization procedure hinges on the implementation of a key cancellation, which proceeds through the judicious combination of the SDE for the three-gluon vertex and the BSE for  $\mathbb{B}(r)$ . It turns out that the mathematical origin of this cancellation may be traced back to Fredholm's alternatives theorem, operating at the level of the SDE-BSE system that we consider. The nonlinear character of the BSE is crucial for evading this theorem, which would otherwise enforce the strict vanishing of the gluon mass.

For the purpose of simplifying this rather technical subject, in our presentation we have considered only the minimum of diagrams required for exposing the crucial cancellations [see Sec. VII] and their connection to Fredholm's theorem. It is, however, of the utmost importance to emphasize that, as we have explicitly confirmed, the omitted contributions undergo themselves completely analogous cancellations, which proceed in exactly the same way, and for precisely the same reason. Actually, the construction related to the renormalization may be repeated, involving the ghost-gluon and four-gluon vertices, their SDE-BSE systems, and the corresponding vertex renormalization constants associated with them. In fact, the only contributions that survive, and may induce modifications to the results presented here originate from the non-linear components of the additional BSEs that control the formation of poles in the ghost-gluon and four-gluon vertices. The detailed elaboration of these issues will be presented in a forthcoming communication.

The numerical treatment presented in Sec. IX focused on two principal quantities, namely the value of the gluon mass,  $m$ , and the shape and size of the displacement function,  $\mathbb{C}(r)$ . The procedure followed consists in producing a sequence of models for  $K(r, k)$ , in an attempt to optimize the resulting set  $\{m, \mathbb{C}(r)\}$  with respect to the lattice-based benchmarks for these quantities. The analysis reveals a preference towards gluon masses that are larger than

what the saturation point of the lattice gluon propagator would indicate. In particular, the red continuous curve in Fig. 15, which shows the best coincidence with the  $\mathbb{C}(r)$  of [76], is obtained for  $m = 687$  MeV, which is to be contrasted to the  $m_{\text{lat}} = 354$  MeV [106]. As we discuss below, there are at least three reasons that could account for this relative tension between  $m$  and  $\mathbb{C}(r)$ .

First, for our numerical analysis we have essentially resorted to models for the kernel, using the one-gluon exchange version as our reference. Evidently, the next important task in this context would be to actually compute the modifications induced to  $K(r, k)$  by the inclusions of the one-loop dressed diagrams  $(b_3)$ - $(b_6)$  appearing in the skeleton expansion of Fig. 9. The result of such a computation is likely to modify the shape of  $\mathbb{B}(r)$ , in ways not captured by the modeling described by Eqs. (9.17) and (9.19), thus improving the matching between  $m$  and  $\mathbb{C}(r)$ . Calculations in this direction are already underway; we hope to report on the results of this study in the near future.

Second, the indirect determination of  $\mathbb{C}(r)$  presented in [76] involves a particular partial derivative of the ghost-gluon kernel,  $H_{\nu\mu}(p, q, r)$ , appearing in the STI of Eq. (3.24). This derivative has never been simulated on the lattice; in the analysis of [76] it was estimated with the aid of the “one-loop dressed” SDE that controls the evolution of  $H_{\nu\mu}(p, q, r)$ . Preliminary analysis indicates that a relatively small change in the functional form of this derivative would suffice for bringing  $m$  and  $\mathbb{C}(r)$  to a closer agreement. It is therefore important to examine the modifications induced to this quantity when further contributions to the SDE are included; in particular, such a study requires the inclusion into the aforementioned SDE of the ghost-ghost-gluon-gluon vertex, first explored in [141].

Third, as mentioned above, the inclusion of the remaining fundamental vertices of the theory, namely the ghost-gluon and four-gluon vertices, is likely to modify the expression for  $I$  given in Eq. (7.1). In particular, the non-linearities in the BSEs that control the formation of the composite scalar through the fusion of a ghost-antighost pair or three gluons will provide additional finite contributions to the  $I$ , thus affecting the value of the gluon mass. The inclusion of the ghost-gluon vertex and the associated pole dynamics is well within our grasp, and various of its main aspects have already been addressed in the literature [49, 58, 59, 75]. On the other hand, the pole content and structure of the four-gluon vertex are largely unexplored, and quantitative information is rather difficult to obtain [73, 142–146]; nonetheless, the understanding acquired from the present analysis is

expected to facilitate future attempts in this direction.

## XI. ACKNOWLEDGMENTS

The work of M. N. F. is supported by the National Natural Science Foundation of China (grant no. 12135007). The research of J. P. is supported by the Spanish MICINN grant PID2020-113334GB-I00, the Generalitat Valenciana grant CIPROM/2022/66, and in part by the EMMI visiting grant of the ExtreMe Matter Institute EMMI at the GSI Helmholtzzentrum für Schwerionenforschung GmbH, Darmstadt, Germany. J. P. thanks J. M. Pawłowski for his kind hospitality at the Institute for Theoretical Physics, University of Heidelberg, where part of this work was completed, and for numerous stimulating discussions.

### Appendix A: A toy model

In this Appendix we present a concrete example of the mathematical construction described in Sec. VII, leading from Eq. (7.3) to Eq. (7.6).

In order to make the analogy with the equations for  $L_{sg}(r)$ ,  $\mathbb{B}(r)$ , and  $I$  as realistic as possible, we use an integration interval from 0 to  $\Lambda^2$ , with  $\Lambda$  an ultraviolet cutoff, which will eventually be taken to infinity.

For simplicity, we consider the case of a separable kernel,  $K(x, y) = A(x)B(y)$ , for which Eq. (7.3) can be solved formally. Then, the symmetry of the kernel under the exchange of  $x$  and  $y$  implies  $B(y) = A(y)$ . Moreover, we set  $u(x) = 1$ . In this case, Eq. (7.3) simplifies to

$$g(x) = z + A(x) \int_0^{\Lambda^2} dy g(y) A(y), \quad f(x) = b^{-1} A(x) \int_0^{\Lambda^2} dy f(y) A(y). \quad (\text{A1})$$

To fix the ideas, let us first ignore convergence issues of the integrals in Eq. (A1) as  $\Lambda \rightarrow \infty$ . Then, the formal solution of Eq. (A1) for  $g(x)$  and  $f(x)$  is read off immediately,

$$g(x) = z + cA(x), \quad f(x) = dA(x), \quad (\text{A2})$$

where  $c$  and  $d$  are so-far unknown constants, defined as

$$c = \int_0^{\Lambda^2} dy g(y) A(y), \quad d = b^{-1} \int_0^{\Lambda^2} dy f(y) A(y). \quad (\text{A3})$$



Next, the constant  $c$  can be determined by substituting Eq. (A2) into the first of Eq. (A3) to eliminate  $g(y)$ . This yields a linear equation for  $c$ , whose solution reads

$$c = z \left[ 1 - \int_0^{\Lambda^2} dw A^2(w) \right]^{-1} \int_0^{\Lambda^2} dy A(y). \quad (\text{A4})$$

On the other hand, substituting Eq. (A2) into the second of Eq. (A3) leads to

$$d = db^{-1} \int_0^{\Lambda^2} dy A^2(y), \quad (\text{A5})$$

which leaves  $d$  undetermined. That is to be expected, since the equation for  $f(x)$  is homogeneous; its solutions can only be determined up to a multiplicative constant. Instead, Eq. (A5) determines  $b$ , which plays the role of eigenvalue. Specifically,

$$b = \int_0^{\Lambda^2} dy A^2(y). \quad (\text{A6})$$

Now we consider the two forms of  $\beta$ , given by Eqs. (7.4) and (7.6). Using Eq. (A2), the Eqs. (7.4) and (7.6) reduce to

$$\beta = z d \int_0^{\Lambda^2} dx A(x), \quad \beta = d(1-b) \int_0^{\Lambda^2} dx A(x)[z + cA(x)]. \quad (\text{A7})$$

Then, using Eqs. (A4) and (A6) for  $c$  and  $b$ , one finds by simple algebra that the two expressions yield the same result.

To make this example more concrete, let  $A(x) = e^{-x}$ . With this kernel, all of the above integrals converge in the limit  $\Lambda \rightarrow \infty$ , which we can take directly. Then, we can set  $z = 1$ , such that Eq. (7.3) reduces to

$$g(x) = 1 + \int_0^{\infty} dy g(y) e^{-x-y}, \quad f(x) = b^{-1} \int_0^{\infty} dy f(y) e^{-x-y}. \quad (\text{A8})$$

The solution is found from Eqs. (A2), (A4), and (A6), which yield  $b = 1/2$ ,  $c = 2$ , and

$$g(x) = 1 + 2e^{-x}, \quad f(x) = de^{-x}, \quad (\text{A9})$$

with  $d$  an undetermined constant. These results are readily verified to satisfy Eq. (A8). Finally, both forms of Eq. (A7) yield  $\beta = d$ .

Now, the actual equations for  $L_{sg}(r)$  and  $\mathbb{B}(r)$  contain ultraviolet divergences that are cured by renormalization. To emulate this situation within our toy model, let us choose

$$A(x) = \frac{a}{x + h^2}, \quad (\text{A10})$$

with  $a$  and  $h$  constant. With this kernel, no infrared divergences arise, but the treatment of the  $\Lambda \rightarrow \infty$  limit requires additional care.

The homogeneous equation for  $f(x)$  does not present a problem; its solution is still given by Eq. (A9), with the ultraviolet finite eigenvalue

$$b = \int_0^{\Lambda^2} dy A^2(y) = \frac{a^2 \Lambda^2}{h^2(\Lambda^2 + h^2)}, \quad \lim_{\Lambda \rightarrow \infty} b = \frac{a^2}{h^2}. \quad (\text{A11})$$

However, if  $z$  were cutoff-independent, say  $z = 1$ , the inhomogeneous equation for  $g(x)$  in Eq. (A1) would lead to a divergent result. Specifically, from Eq. (A4),

$$c = \frac{ah^2(\Lambda^2 + h^2)}{(h^2 - a^2)\Lambda^2 + h^4} \ln \left( \frac{\Lambda^2 + h^2}{h^2} \right), \quad (\text{A12})$$

such that

$$\lim_{\Lambda \rightarrow \infty} c = \frac{ah^2}{h^2 - a^2} \ln \left( \frac{\Lambda^2}{h^2} \right), \quad (\text{A13})$$

*i.e.*,  $c$ , and therefore  $g(x)$ , diverge logarithmically, in close analogy to the unrenormalized  $L_{sg}(x)$ .

Let us then choose  $z$  in Eq. (A1) to be cutoff-dependent, in such a way that it cancels the divergence of the integral in the equation for  $g(x)$ . To this end, we impose a ‘‘renormalization condition’’,  $g(\mu^2) = 1$ , at some renormalization point,  $\mu^2$ . This condition determines  $z$  as

$$z = 1 - A(\mu^2) \int_0^{\Lambda^2} dy g(y) A(y). \quad (\text{A14})$$

Then, the first of Eq. (7.3) becomes

$$g(x) = 1 + [A(x) - A(\mu^2)] \int_0^{\Lambda^2} dy g(y) A(y), \quad (\text{A15})$$

while the equation for  $f(x)$  is unchanged.

The solution of the system is reached through the same steps used to obtain Eqs. (A2) and (A3). Specifically, we find

$$g(x) = 1 + c_R[A(x) - A(\mu^2)], \quad f(x) = d_R A(x), \quad (\text{A16})$$

with

$$\begin{aligned} c_R &= \left\{ 1 - \int_0^{\Lambda^2} dw A(w) [A(w) - A(\mu^2)] \right\}^{-1} \int_0^{\Lambda^2} dy A(y) \\ &= \frac{ah^2(\Lambda^2 + h^2)(\mu^2 + h^2) \ln(1 + \Lambda^2/h^2)}{(\mu^2 + h^2)[\Lambda^2(h^2 - a^2) + h^4] + a^2 h^2(\Lambda^2 + h^2) \ln(1 + \Lambda^2/h^2)}, \end{aligned} \quad (\text{A17})$$

$d_{\text{R}}$  arbitrary, and the eigenvalue  $b$  given by Eq. (A11).

Now, the constant  $c_{\text{R}}$ , and hence  $g(x)$ , is finite. In fact, for  $\Lambda \rightarrow \infty$ ,  $c_{\text{R}}$  takes the simple form

$$\lim_{\Lambda \rightarrow \infty} c_{\text{R}} = \frac{\mu^2 + h^2}{a}. \quad (\text{A18})$$

Next, we consider the two expressions for  $\beta$  in Eq. (A7). To calculate the first form, we first need to know the explicit value of  $z$ ; this is achieved by substituting the solution given in Eqs. (A16) and (A17) for  $g(x)$  into Eq. (A14), which furnishes

$$z = \frac{(\mu^2 + h^2) [\Lambda^2(h^2 - a^2) + h^4]}{(\mu^2 + h^2) [\Lambda^2(h^2 - a^2) + h^4] + a^2 h^2 (\Lambda^2 + h^2) \ln(1 + \Lambda^2/h^2)}. \quad (\text{A19})$$

Then, with a little algebra, both expressions in Eq. (A7) can be shown to yield the same result, namely

$$\beta = \frac{ad(\mu^2 + h^2) [\Lambda^2(h^2 - a^2) + h^4] \ln(1 + \Lambda^2/h^2)}{(\mu^2 + h^2) [\Lambda^2(h^2 - a^2) + h^4] + a^2 h^2 (\Lambda^2 + h^2) \ln(1 + \Lambda^2/h^2)}, \quad (\text{A20})$$

which for  $\Lambda \rightarrow \infty$  has the finite value

$$\lim_{\Lambda \rightarrow \infty} \beta = \frac{d(\mu^2 + h^2)(h^2 - a^2)}{ah^2}. \quad (\text{A21})$$

We conclude this exercise by considering the scale-fixing of the homogeneous equation; this can be achieved by imposing an additional relation between  $b$  and  $f$ .

To retain a close analogy with the situation encountered in the equations for  $\mathbb{B}(r)$ , we recall that, in our toy model,  $b$  plays the role of the  $t$  appearing in Eq. (5.15). Then, by analogy to Eq. (5.10), we impose that  $b$  must satisfy

$$b = 1 - \int_0^{\Lambda^2} dy f^2(y), \quad (\text{A22})$$

with the integral on the r.h.s. emulating the  $\omega$  of Eq. (5.10). Note that since Eq. (A22) is quadratic in  $f(y)$ , Eqs. (A10) and (A16) yield an ultraviolet finite  $b$ , namely

$$b = 1 - \frac{d_{\text{R}}^2 a^2 \Lambda^2}{h^2 (\Lambda^2 + h^2)}, \quad \lim_{\Lambda \rightarrow \infty} b = 1 - \frac{d_{\text{R}}^2 a^2}{h^2}. \quad (\text{A23})$$

Now, Eqs. (A11) and (A23) must yield the same value of  $b$ . Hence, equating them fixes the scale of  $d_{\text{R}}$  to

$$d_{\text{R}} = \pm \sqrt{\frac{h^2 (\Lambda^2 + h^2)}{a^2 \Lambda^2} - 1}, \quad \lim_{\Lambda \rightarrow \infty} d_{\text{R}} = \pm \sqrt{\frac{h^2}{a^2} - 1}. \quad (\text{A24})$$

Since Eq. (A22) is quadratic in  $f(y)$ , the sign of  $d_R$  is left undetermined, similarly to the sign of  $\sigma$  in Eq. (6.13).

- 
- [1] C.-N. Yang and R. L. Mills, *Phys. Rev.* **96**, 191 (1954).
  - [2] D. J. Gross and F. Wilczek, *Phys. Rev. Lett.* **30**, 1343 (1973).
  - [3] H. D. Politzer, *Phys. Rev. Lett.* **30**, 1346 (1973).
  - [4] W. J. Marciano and H. Pagels, *Phys. Rept.* **36**, 137 (1978).
  - [5] L. D. Faddeev and V. N. Popov, *Phys. Lett. B* **25**, 29 (1967).
  - [6] C. Becchi, A. Rouet, and R. Stora, *Commun. Math. Phys.* **42**, 127 (1975).
  - [7] I. V. Tyutin, LEBEDEV-75-39 (1975).
  - [8] C. Becchi, A. Rouet, and R. Stora, *Annals Phys.* **98**, 287 (1976).
  - [9] G. 't Hooft and M. J. G. Veltman, *Nucl. Phys. B* **44**, 189 (1972).
  - [10] C. G. Bollini and J. J. Giambiagi, *Nuovo Cim. B* **12**, 20 (1972).
  - [11] J. M. Cornwall, *Phys. Rev. D* **26**, 1453 (1982).
  - [12] J. S. Schwinger, *Phys. Rev.* **125**, 397 (1962).
  - [13] J. S. Schwinger, *Phys. Rev.* **128**, 2425 (1962).
  - [14] E. Eichten and F. Feinberg, *Phys. Rev. D* **10**, 3254 (1974).
  - [15] J. Smit, *Phys. Rev. D* **10**, 2473 (1974).
  - [16] G. Parisi and R. Petronzio, *Phys. Lett. B* **94**, 51 (1980).
  - [17] C. W. Bernard, *Phys. Lett. B* **108**, 431 (1982).
  - [18] C. W. Bernard, *Nucl. Phys. B* **219**, 341 (1983).
  - [19] J. F. Donoghue, *Phys. Rev. D* **29**, 2559 (1984).
  - [20] J. Mandula and M. Ogilvie, *Phys. Lett. B* **185**, 127 (1987).
  - [21] J. M. Cornwall and J. Papavassiliou, *Phys. Rev. D* **40**, 3474 (1989).
  - [22] M. Lavelle, *Phys. Rev. D* **44**, 26 (1991).
  - [23] F. Halzen, G. I. Krein, and A. A. Natale, *Phys. Rev. D* **47**, 295 (1993).
  - [24] K. G. Wilson, T. S. Walhout, A. Harindranath, W.-M. Zhang, R. J. Perry, and S. D. Glazek, *Phys. Rev.* **D49**, 6720 (1994).
  - [25] A. Mihara and A. A. Natale, *Phys. Lett. B* **482**, 378 (2000).
  - [26] K.-I. Kondo, *Phys. Lett. B* **514**, 335 (2001).

- [27] O. Philipsen, [Nucl. Phys. \*\*B628\*\*, 167 \(2002\)](#).
- [28] A. C. Aguilar, A. A. Natale, and P. S. Rodrigues da Silva, [Phys. Rev. Lett. \*\*90\*\*, 152001 \(2003\)](#).
- [29] J. M. Pawłowski, D. F. Litim, S. Nedelko, and L. von Smekal, [Phys. Rev. Lett. \*\*93\*\*, 152002 \(2004\)](#).
- [30] A. C. Aguilar and A. A. Natale, [JHEP \*\*08\*\*, 057 \(2004\)](#).
- [31] A. C. Aguilar and J. Papavassiliou, [JHEP \*\*12\*\*, 012 \(2006\)](#).
- [32] D. Epple, H. Reinhardt, W. Schleifenbaum, and A. P. Szczepaniak, [Phys. Rev. \*\*D77\*\*, 085007 \(2008\)](#).
- [33] A. C. Aguilar, D. Binosi, and J. Papavassiliou, [Phys. Rev. \*\*D78\*\*, 025010 \(2008\)](#).
- [34] J. Braun, H. Gies, and J. M. Pawłowski, [Phys. Lett. \*\*B684\*\*, 262 \(2010\)](#).
- [35] M. Tissier and N. Wschebor, [Phys. Rev. D \*\*82\*\*, 101701 \(2010\)](#).
- [36] D. R. Campagnari and H. Reinhardt, [Phys. Rev. \*\*D82\*\*, 105021 \(2010\)](#).
- [37] M. Tissier and N. Wschebor, [Phys. Rev. \*\*D84\*\*, 045018 \(2011\)](#).
- [38] J. Serreau and M. Tissier, [Phys. Lett. \*\*B712\*\*, 97 \(2012\)](#).
- [39] D. A. Fagundes, E. G. S. Luna, M. J. Menon, and A. A. Natale, [Nucl. Phys. A \*\*886\*\*, 48 \(2012\)](#).
- [40] D. Binosi, D. Ibañez, and J. Papavassiliou, [Phys. Rev. \*\*D86\*\*, 085033 \(2012\)](#).
- [41] A. Maas, [Phys. Rept. \*\*524\*\*, 203 \(2013\)](#).
- [42] F. Siringo, [Nucl. Phys. \*\*B907\*\*, 572 \(2016\)](#).
- [43] A. K. Cyrol, L. Fister, M. Mitter, J. M. Pawłowski, and N. Strodthoff, [Phys. Rev. \*\*D94\*\*, 054005 \(2016\)](#).
- [44] S. D. Glazek, M. Gómez-Rocha, J. More, and K. Serafin, [Phys. Lett. \*\*B773\*\*, 172 \(2017\)](#).
- [45] A. K. Cyrol, J. M. Pawłowski, A. Rothkopf, and N. Wink, [SciPost Phys. \*\*5\*\*, 065 \(2018\)](#).
- [46] J. A. Gracey, M. Peláez, U. Reinosa, and M. Tissier, [Phys. Rev. D \*\*100\*\*, 034023 \(2019\)](#).
- [47] C. D. Roberts, [Symmetry \*\*12\*\*, 1468 \(2020\)](#).
- [48] M. Peláez, U. Reinosa, J. Serreau, M. Tissier, and N. Wschebor, [Rept. Prog. Phys. \*\*84\*\*, 124202 \(2021\)](#).
- [49] G. Eichmann, J. M. Pawłowski, and J. a. M. Silva, [Phys. Rev. D \*\*104\*\*, 114016 \(2021\)](#).
- [50] J. Horak, F. Ihssen, J. Papavassiliou, J. M. Pawłowski, A. Weber, and C. Wetterich, [SciPost Phys. \*\*13\*\*, 042 \(2022\)](#).

- [51] J. Papavassiliou, [Chin. Phys. C \*\*46\*\*, 112001 \(2022\)](#).
- [52] M. Ding, C. D. Roberts, and S. M. Schmidt, [Particles \*\*6\*\*, 57 \(2023\)](#).
- [53] M. N. Ferreira and J. Papavassiliou, [Particles \*\*6\*\*, 312 \(2023\)](#).
- [54] E. C. Poggio, E. Tomboulis, and S. H. H. Tye, [Phys. Rev. \*\*D11\*\*, 2839 \(1975\)](#).
- [55] A. C. Aguilar, D. Ibanez, V. Mathieu, and J. Papavassiliou, [Phys. Rev. \*\*D85\*\*, 014018 \(2012\)](#).
- [56] D. Ibañez and J. Papavassiliou, [Phys. Rev. \*\*D87\*\*, 034008 \(2013\)](#).
- [57] A. C. Aguilar, D. Binosi, and J. Papavassiliou, [Front. Phys.\(Beijing\) \*\*11\*\*, 111203 \(2016\)](#).
- [58] A. C. Aguilar, D. Binosi, C. T. Figueiredo, and J. Papavassiliou, [Eur. Phys. J. \*\*C78\*\*, 181 \(2018\)](#).
- [59] A. C. Aguilar, M. N. Ferreira, and J. Papavassiliou, [Phys. Rev. D \*\*105\*\*, 014030 \(2022\)](#).
- [60] C. D. Roberts and A. G. Williams, [Prog. Part. Nucl. Phys. \*\*33\*\*, 477 \(1994\)](#).
- [61] R. Alkofer and L. von Smekal, [Phys. Rept. \*\*353\*\*, 281 \(2001\)](#).
- [62] P. Maris and C. D. Roberts, [Int. J. Mod. Phys. \*\*E12\*\*, 297 \(2003\)](#).
- [63] C. S. Fischer, [J. Phys. G \*\*32\*\*, R253 \(2006\)](#).
- [64] C. D. Roberts, [Prog. Part. Nucl. Phys. \*\*61\*\*, 50 \(2008\)](#).
- [65] C. S. Fischer, A. Maas, and J. M. Pawłowski, [Annals Phys. \*\*324\*\*, 2408 \(2009\)](#).
- [66] D. Binosi and J. Papavassiliou, [Phys. Rept. \*\*479\*\*, 1 \(2009\)](#).
- [67] A. Bashir, L. Chang, I. C. Cloet, B. El-Bennich, Y.-X. Liu, *et al.*, [Commun. Theor. Phys. \*\*58\*\*, 79 \(2012\)](#).
- [68] L. Fister and J. M. Pawłowski, [Phys. Rev. \*\*D88\*\*, 045010 \(2013\)](#).
- [69] I. C. Cloet and C. D. Roberts, [Prog. Part. Nucl. Phys. \*\*77\*\*, 1 \(2014\)](#).
- [70] D. Binosi, L. Chang, J. Papavassiliou, and C. D. Roberts, [Phys. Lett. \*\*B742\*\*, 183 \(2015\)](#).
- [71] D. Binosi, L. Chang, J. Papavassiliou, S.-X. Qin, and C. D. Roberts, [Phys. Rev. \*\*D93\*\*, 096010 \(2016\)](#).
- [72] D. Binosi, C. Mezrag, J. Papavassiliou, C. D. Roberts, and J. Rodriguez-Quintero, [Phys. Rev. \*\*D96\*\*, 054026 \(2017\)](#).
- [73] M. Q. Huber, [Phys. Rept. \*\*879\*\*, 1 \(2020\)](#).
- [74] M. Q. Huber, [Phys. Rev. D \*\*101\*\*, 114009 \(2020\)](#).
- [75] A. C. Aguilar, D. Binosi, C. T. Figueiredo, and J. Papavassiliou, [Phys. Rev. \*\*D94\*\*, 045002 \(2016\)](#).
- [76] A. C. Aguilar, F. De Soto, M. N. Ferreira, J. Papavassiliou, F. Pinto-Gómez, C. D. Roberts,

- and J. Rodríguez-Quintero, *Phys. Lett. B* **841**, 137906 (2023).
- [77] C. Alexandrou, P. de Forcrand, and E. Follana, *Phys. Rev. D* **65**, 114508 (2002).
- [78] A. Cucchieri and T. Mendes, *PoS LATTICE2007*, 297 (2007).
- [79] I. Bogolubsky, E. Ilgenfritz, M. Muller-Preussker, and A. Sternbeck, *PoS LATTICE2007*, 290 (2007).
- [80] P. O. Bowman, U. M. Heller, D. B. Leinweber, M. B. Parappilly, A. Sternbeck, L. von Smekal, A. G. Williams, and J.-b. Zhang, *Phys. Rev. D* **76**, 094505 (2007).
- [81] W. Kamleh, P. O. Bowman, D. B. Leinweber, A. G. Williams, and J. Zhang, *Phys. Rev. D* **76**, 094501 (2007).
- [82] A. Cucchieri and T. Mendes, *Phys. Rev. Lett.* **100**, 241601 (2008).
- [83] I. Bogolubsky, E. Ilgenfritz, M. Muller-Preussker, and A. Sternbeck, *Phys. Lett.* **B676**, 69 (2009).
- [84] O. Oliveira and P. Silva, *PoS LAT2009*, 226 (2009).
- [85] A. Cucchieri, T. Mendes, and E. M. S. Santos, *Phys. Rev. Lett.* **103**, 141602 (2009).
- [86] A. Cucchieri and T. Mendes, *Phys. Rev.* **D81**, 016005 (2010).
- [87] A. Cucchieri, T. Mendes, G. M. Nakamura, and E. M. S. Santos, *PoS FACESQCD*, 026 (2010).
- [88] O. Oliveira and P. Bicudo, *J. Phys. G* **G38**, 045003 (2011).
- [89] A. Ayala, A. Bashir, D. Binosi, M. Cristoforetti, and J. Rodríguez-Quintero, *Phys. Rev.* **D86**, 074512 (2012).
- [90] A. Sternbeck and M. Müller-Preussker, *Phys. Lett. B* **726**, 396 (2013).
- [91] P. Bicudo, D. Binosi, N. Cardoso, O. Oliveira, and P. J. Silva, *Phys. Rev.* **D92**, 114514 (2015).
- [92] A. G. Duarte, O. Oliveira, and P. J. Silva, *Phys. Rev. D* **94**, 014502 (2016).
- [93] D. Dudal, O. Oliveira, and P. J. Silva, *Annals Phys.* **397**, 351 (2018).
- [94] A. C. Aguilar, F. De Soto, M. N. Ferreira, J. Papavassiliou, J. Rodríguez-Quintero, and S. Zafeiropoulos, *Eur. Phys. J.* **C80**, 154 (2020).
- [95] A. C. Aguilar, M. . N. Ferreira, D. Ibañez, and J. Papavassiliou, *Eur. Phys. J. C* **83**, 967 (2023).
- [96] V. Vladimirov, *Equations of Mathematical Physics*, Monographs and textbooks in pure and applied mathematics (M. Dekker, 1971).

- [97] A. Polyanin and A. Manzhirov, *Handbook of Integral Equations: Second Edition* (Taylor & Francis, 2008).
- [98] B. Zumino, *Acta Phys. Austriaca Suppl.* **2**, 212 (1965).
- [99] R. Jackiw and K. Johnson, *Phys. Rev. D* **8**, 2386 (1973).
- [100] R. Jackiw, *Proceedings, Laws Of Hadronic Matter, Erice*, (MIT, Cambridge, MA, 1973).
- [101] J. Cornwall and R. Norton, *Phys. Rev. D* **8**, 3338 (1973).
- [102] A. Athenodorou, D. Binosi, P. Boucaud, F. De Soto, J. Papavassiliou, J. Rodríguez-Quintero, and S. Zafeiropoulos, *Phys. Lett.* **B761**, 444 (2016).
- [103] P. Boucaud, F. De Soto, J. Rodríguez-Quintero, and S. Zafeiropoulos, *Phys. Rev.* **D95**, 114503 (2017).
- [104] A. Sternbeck, P.-H. Balduf, A. Kizilersu, O. Oliveira, P. J. Silva, J.-I. Skullerud, and A. G. Williams, *PoS LATTICE2016*, 349 (2017).
- [105] A. C. Aguilar, F. De Soto, M. N. Ferreira, J. Papavassiliou, and J. Rodríguez-Quintero, *Phys. Lett. B* **818**, 136352 (2021).
- [106] A. C. Aguilar, C. O. Ambrósio, F. De Soto, M. N. Ferreira, B. M. Oliveira, J. Papavassiliou, and J. Rodríguez-Quintero, *Phys. Rev. D* **104**, 054028 (2021).
- [107] A. Maas and M. Vujanović, *SciPost Phys. Core* **5**, 019 (2022).
- [108] G. T. R. Catumba, O. Oliveira, and P. J. Silva, *PoS LATTICE2021*, 467 (2022).
- [109] G. T. R. Catumba, O. Oliveira, and P. J. Silva, *EPJ Web Conf.* **258**, 02008 (2022).
- [110] F. Pinto-Gómez, F. De Soto, M. N. Ferreira, J. Papavassiliou, and J. Rodríguez-Quintero, *Phys. Lett. B* **838**, 137737 (2023).
- [111] J. Berges, *Phys. Rev. D* **70**, 105010 (2004).
- [112] M. E. Carrington and Y. Guo, *Phys. Rev. D* **83**, 016006 (2011).
- [113] M. C. A. York, G. D. Moore, and M. Tassler, *JHEP* **06**, 077 (2012).
- [114] N. Mueller and J. M. Pawłowski, *Phys. Rev.* **D91**, 116010 (2015).
- [115] R. Williams, C. S. Fischer, and W. Heupel, *Phys. Rev.* **D93**, 034026 (2016).
- [116] A. C. Aguilar, M. N. Ferreira, J. Papavassiliou, and L. R. Santos, *Eur. Phys. J. C* **83**, 549 (2023).
- [117] M. Q. Huber, C. S. Fischer, and H. Sanchis-Alepuz, *Eur. Phys. J. C* **80**, 1077 (2020).
- [118] M. Q. Huber, C. S. Fischer, and H. Sanchis-Alepuz, *Eur. Phys. J. C* **81**, 1083 (2021), [Erratum: *Eur.Phys.J.C* 82, 38 (2022)].



- [119] J. Taylor, [Nucl. Phys. B \*\*33\*\*, 436 \(1971\)](#).
- [120] A. Slavnov, [Theor. Math. Phys. \*\*10\*\*, 99 \(1972\)](#).
- [121] A. C. Aguilar, M. N. Ferreira, B. M. Oliveira, J. Papavassiliou, and L. R. Santos, [Eur. Phys. J. C \*\*83\*\*, 889 \(2023\)](#).
- [122] J. S. Ball and T.-W. Chiu, [Phys. Rev. D \*\*22\*\*, 2550 \(1980\)](#), [Erratum: Phys. Rev. D 23, 3085 (1981)].
- [123] A. I. Davydychev, P. Osland, and O. Tarasov, [Phys. Rev. D \*\*54\*\*, 4087 \(1996\)](#), [Erratum: Phys. Rev. D 59, 109901 (1999)].
- [124] J. Gracey, H. Kißler, and D. Kreimer, [Phys. Rev. D \*\*100\*\*, 085001 \(2019\)](#).
- [125] A. C. Aguilar, D. Binosi, and J. Papavassiliou, [Phys. Rev. \*\*D89\*\*, 085032 \(2014\)](#).
- [126] J. D. Bjorken and S. D. Drell, *Relativistic quantum fields*, International Series In Pure and Applied Physics (McGraw-Hill, New York, 1965).
- [127] Z.-F. Cui, J.-L. Zhang, D. Binosi, F. de Soto, C. Mezrag, J. Papavassiliou, C. D. Roberts, J. Rodríguez-Quintero, J. Segovia, and S. Zafeiropoulos, [Chin. Phys. C \*\*44\*\*, 083102 \(2020\)](#).
- [128] G. Eichmann, R. Williams, R. Alkofer, and M. Vujanovic, [Phys. Rev. \*\*D89\*\*, 105014 \(2014\)](#).
- [129] A. Blum, M. Q. Huber, M. Mitter, and L. von Smekal, [Phys. Rev. \*\*D89\*\*, 061703 \(2014\)](#).
- [130] M. Mitter, J. M. Pawłowski, and N. Strodthoff, [Phys. Rev. \*\*D91\*\*, 054035 \(2015\)](#).
- [131] J. M. Pawłowski, C. S. Schneider, and N. Wink, [arXiv:2202.11123 \[hep-th\] \(2022\)](#).
- [132] W. H. Press, S. A. Teukolsky, W. T. Vetterling, and B. P. Flannery, *Numerical Recipes in FORTRAN: The Art of Scientific Computing* (Cambridge University Press, 1992).
- [133] G. Altarelli, [Phys. Rept. \*\*81\*\*, 1 \(1982\)](#).
- [134] L. von Smekal, A. Hauck, and R. Alkofer, [Annals Phys. \*\*267\*\*, 1 \(1998\)](#), [Erratum: Annals Phys. 269, 182 (1998)].
- [135] C. S. Fischer, R. Alkofer, and H. Reinhardt, [Phys. Rev. D \*\*65\*\*, 094008 \(2002\)](#).
- [136] M. R. Pennington and D. J. Wilson, [Phys. Rev. \*\*D84\*\*, 119901 \(2011\)](#).
- [137] W. Celmaster and R. J. Gonsalves, [Phys. Rev. Lett. \*\*42\*\*, 1435 \(1979\)](#).
- [138] W. Celmaster and R. J. Gonsalves, [Phys. Rev. D \*\*20\*\*, 1420 \(1979\)](#).
- [139] B. Alles, D. Henty, H. Panagopoulos, C. Parrinello, C. Pittori, and D. G. Richards, [Nucl. Phys. \*\*B502\*\*, 325 \(1997\)](#).
- [140] P. Boucaud, F. De Soto, J. Leroy, A. Le Yaouanc, J. Micheli, *et al.*, [Phys. Rev. \*\*D79\*\*, 014508 \(2009\)](#).

- [141] M. Q. Huber, [Eur. Phys. J. C77](#), 733 (2017).
- [142] D. Binosi, D. Ibañez, and J. Papavassiliou, [JHEP 09](#), 059 (2014).
- [143] A. K. Cyrol, M. Q. Huber, and L. von Smekal, [Eur. Phys. J. C75](#), 102 (2015).
- [144] J. M. Pawłowski, C. S. Schneider, J. Turnwald, J. M. Urban, and N. Wink, [Phys. Rev. D 108](#), 076018 (2023).
- [145] M. Colaço, O. Oliveira, and P. J. Silva, [Phys. Rev. D 109](#), 074502 (2024).
- [146] A. C. Aguilar, M. N. Ferreira, J. Papavassiliou, and L. R. Santos, [arXiv:2402.16071 \[hep-ph\]](#) (2024).